ANNUAL REVIEWS

*Annual Review of Marine Science*

# Oil Transport Following the *Deepwater Horizon* Blowout

Michel C. Boufadel,[1] Tamay Özgökmen,[2] Scott A. Socolofsky,[3] Vassiliki H. Kourafalou,[2] Ruixue Liu,[1] and Kenneth Lee[4]

[1]Center for Natural Resources, Department of Civil and Environmental Engineering, New Jersey Institute of Technology, Newark, New Jersey, USA; email: boufadel@gmail.com

[2]Rosentiel School of Marine and Atmospheric Science, University of Miami, Miami, Florida, USA

[3]Zachry Department of Civil Engineering, Texas A&M University, College Station, Texas, USA

[4]Bedford Institute of Oceanography, Fisheries and Oceans Canada, Dartmouth, Nova Scotia, Canada

ANNUAL REVIEWS CONNECT

www.annualreviews.org

- Download figures
- Navigate cited references
- Keyword search
- Explore related articles
- Share via email or social media

Annu. Rev. Mar. Sci. 2023. 15:67–93

First published as a Review in Advance on June 30, 2022

The *Annual Review of Marine Science* is online at marine.annualreviews.org

https://doi.org/10.1146/annurev-marine-040821-104411

Copyright © 2023 by the author(s). This work is licensed under a Creative Commons Attribution 4.0 International License, which permits unrestricted use, distribution, and reproduction in any medium, provided the original author and source are credited. See credit lines of images or other third-party material in this article for license information.

OPEN ACCESS CC BY

## Keywords

oil spreading, dispersion, droplet formation, eddy diffusivity

## Abstract

The *Deepwater Horizon* oil spill in the Gulf of Mexico in 2010 was the largest in US history, covering more than 1,000 km of shorelines and causing losses that exceeded $50 billion. While oil transformation processes are understood at the laboratory scale, the extent of the *Deepwater Horizon* spill made it challenging to integrate these processes in the field. This review tracks the *Deepwater Horizon* oil during its journey from the Mississippi Canyon block 252 (MC252) wellhead, first discussing the formation of the oil and gas plume and the ensuing oil droplet size distribution, then focusing on the behavior of the oil on the water surface with and without waves. It then reports on massive drifter experiments in the Gulf of Mexico and the impact of the Mississippi River on the oil transport. Finally, it concludes by addressing the formation of oil–particle aggregates. Although physical processes lend themselves to numerical modeling, we attempted to elucidate them without using advanced modeling, as our goal is to enhance communication among scientists, engineers, and other entities interested in oil spills.

## 1. INTRODUCTION

The *Deepwater Horizon* spill was characterized by 87 days of continuous release of oil at the seabed of the Gulf of Mexico (Gros et al. 2017, McNutt et al. 2011) and subsequent travel of that oil in the water column, eventually reaching the sea surface (Paris et al. 2012), seabed (Valentine et al. 2014), and shorelines (Michel et al. 2013). Studies have addressed various aspects of the spill, such as biodegradation (Hazen et al. 2016), weathering (Aeppli et al. 2012), and interaction with organic matter in the water column (Dissanayake et al. 2018a, Passow & Overton 2021), as well as the models adopted to represent these fate processes (Spaulding 2017). Numerous challenges emerged when attempting to tackle the problem and reliably evaluate the trajectory and fate of the oil, including limited knowledge of multiphase plume dynamics and the subsequent oil droplet and gas formation from a large orifice (0.5 m) at great depth (1.5 km), the impact of dispersants on such a release, the lack of sufficiently detailed hydrodynamic simulations along with the lack of continuous velocity measurements below 1,100-m depth, and limited knowledge regarding the quantification of the interaction of the oil with suspended sediments in the coastal zone. The present review attempts to address these challenges from a physical oceanography point of view. It addresses the behavior of oil slicks, the formation of oil droplets, the impact of dispersants, and the formation of oil–particle aggregates.

## 2. OIL BEHAVIOR AND DROPLET FORMATION

The movement of an oil slick on a calm water surface was explained through studies in the late 1960s and early 1970s by Fay (1969) and Hoult (1972) using a hypothetical scenario of instantaneous release. In their approach, the spreading of oil follows three phases, each involving different major forces. The initial phase, called gravity–inertia, lasts minutes to a few hours; the oil spreads due to its potential energy, because its buoyancy makes it float on top of the surrounding water (an effect referred to as gravity in this approach). The resisting force is due to inertia as the oil accelerates from rest. The second phase is called gravity–viscous because the resisting force to spreading is the viscosity of the water due to the formation of a boundary layer in the water underneath the oil. The third phase is called surface tension–viscous because the surface tension of the oil–water interface becomes the major force in spreading the oil, while the viscosity of water resists the spreading. An extension of the third phase is the formation of sheens, which are less than a few micrometers thick and thus could cover large areas. As sheens have small volumes, ignoring them does not impact the overall oil budget, but their spatial extent could constitute a major exposure pathway for fauna frequenting the water surface, such as birds (Short et al. 2017) and dolphins (NRC 2013).

The spreading due to the Fay–Hoult framework elucidates major forces but does not have great practical value for a variety of reasons. First, this approach applies to oil spilled directly onto the water from a vessel and not to oil that rises to the surface from below, such as the case of the *Deepwater Horizon* spill. Second, it assumes spreading during calm seas, which is a rare situation. When wind and waves are present, the oil slick breaks into smaller spills (spillets), with characteristic sizes of meters to hundreds of meters, and thus it does not persist as one huge slick, as surmised by Fay and Hoult. In addition, in the presence of breaking waves, the oil slick in each spillet is likely to be torn and transported into the water column to form oil droplets (Liu et al. 2022), whose subsequent transport is different from that of the surface slick. Therefore, oil droplet formation is critical for understanding the trajectory and fate of oil spills.

Regardless of whether the oil on the water surface is entrained into the water column or whether oil emanates from an underwater orifice, oil droplets form because petroleum fluids are immiscible. Thus, an interface between a released oil (and gas) and the ambient seawater

quickly destabilizes, creating a spectrum of oil droplets (in addition to gas bubbles, in the case of an underwater release).

The formation of oil droplets from jets or from a slick on the water depends on the forces causing the breakup and those resisting it. The forces causing the oil droplet breakup are dynamic stresses due to turbulence (Baldyga & Podgórska 1998, Boufadel et al. 2020b, Hinze 1955), and the main resisting force is the oil–water interfacial tension, which typically ranges from 0.02 to 0.035 N/m, a few times lower than the air–water surface tension of 0.07 N/m. The formation or stability of a droplet of size $d$ can be captured through the value of the Weber number, $We$, which represents the ratio of the turbulence-causing breakage forces to the resisting force of the interfacial tension:

$$We = \frac{\rho_c u'^2 d}{\sigma}, \qquad 1.$$

where $\rho_c$ is the density of the continuous fluid (water herein), $u'$ is the root mean square turbulence velocity, and $\sigma$ is the oil–water interfacial tension. A large Weber number (usually >10) leads to droplet breakup. The oil's viscosity also resists breakup, especially when it is large (Calabrese et al. 1986, Hinze 1955) and/or if one uses a dispersant that reduces the interfacial tension (NRC 2019). In such cases, a Weber number that incorporates the impact of oil viscosity—referred to as a modified Weber number (Calabrese et al. 1986, Johansen et al. 2013)—could be used to interpret the oil droplet sizes. Correlations have been developed to obtain a characteristic diameter of the oil, such as the volume mean diameter, $d_{50}$, based on the Weber and Reynolds numbers (Johansen et al. 2013, Z. Li et al. 2017). These approaches have a strong physical underpinning but do not provide the full oil droplet size distribution, which can only be obtained using droplet population models, such as the VDROP model (Zhao et al. 2014, 2015), which provides the oil droplet size distribution in a select control volume for given oil properties and mixing energy in that volume. VDROP was specifically developed to address situations where dispersant is used and the oil's viscosity becomes the main resisting force (hence the letter V in the name). For underwater jets and plumes, Zhao et al. (2014, 2015, 2017b) combined VDROP with correlation equations describing the hydrodynamics of vertical plumes to produce the model VDROP-J, which predicts the oil droplet size distribution and the gas bubble size distribution from underwater releases.

The presence of gas in the pipe could have a major impact on the oil droplet size distribution; using measurements of the gas-to-oil ratio at the wellhead (Reddy et al. 2012), Boufadel et al. (2018b) showed that the Mississippi Canyon block 252 (MC252) *Deepwater Horizon* well had a churn flow regime, in which oil and gas tumble within the pipe with a very large energy dissipation rate, resulting in small oil droplets in comparison with those in a bubbly flow regime or a regime without gas. Recent laboratory work under high pressure suggests that the effervescence of gas due to a rapid release from an orifice could further reduce the oil droplet size distribution (Malone et al. 2018, Pesch et al. 2020). However, the extent of fragmentation is still a topic of debate (Gros et al. 2020). A review of the research on underwater oil and gas release, including some works on the *Deepwater Horizon* riser (pipe), was recently published (Boufadel et al. 2020b).

## 3. MULTIPHASE PLUME DYNAMICS

The subsea blowout of *Deepwater Horizon* involved a high flux of oil and gas released from localized sources, including a kink in the riser lying on the floor; the end of the riser, which was approximately 200 m from the wellhead; and eventually the wellhead itself, after the riser was pared (French-McCay et al. 2015). The releases from these sources quickly evolved to behave as a multiphase plume. In the immediate vicinity of the release, the flow rapidly transitioned through the zone of flow establishment from pipe-flow-type turbulence to a self-similar buoyant jet profile

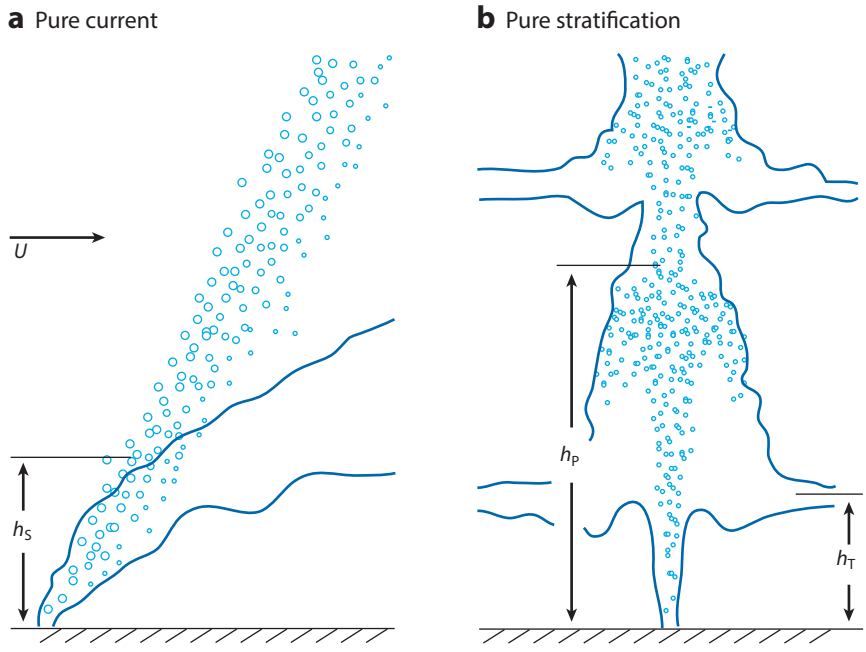


**Figure 1**

Behavior of droplets and bubbles within plumes exposed to (*a*) pure current and (*b*) pure stratification. Note the formation of the intrusion layers in panel *b*, the first at height $h_T$. Figure adapted with permission from Socolofsky et al. (2011).

(Lee & Chu 2003). Within this region, entrainment of ambient seawater violently mixed with the oil and gas, allowing for breakup into gas bubbles and oil droplets (see Section 2). Above the zone of flow establishment, the flow behaved like that of a buoyant, multiphase jet of gas bubbles, oil droplets, and entrained ambient seawater.

Multiphase jets and plumes can be very different from their single-phase counterparts because immiscible bubbles and droplets that provide buoyancy to the buoyant jet might not follow the entrained continuous-phase ambient fluid; instead, they may separate from the jet or plume when their buoyant rise velocity no longer follows the trajectory of the entrained water (**Figure 1*a***). For a plume in stratified ambient conditions (**Figure 1*b***), once the entrained seawater comes to rest above the point of neutral buoyancy, it peels from the rising plume and falls to the level of neutral buoyancy, forming a horizontal intrusion layer at the height $h_T$. Additional intrusion layers could form, as illustrated in **Figure 1*b***. The first intrusion layer of the *Deepwater Horizon* blowout was evident in the stratification profile between 300 and 400 m above the seafloor (Boufadel et al. 2020b).

Most gas bubbles and larger oil droplets will rise out of the top of the plume, not following the descending flow on the outer edge of the plume. Only dissolved hydrocarbon species and smaller oil droplets will proceed into the intrusion layer. For the *Deepwater Horizon*, oil droplets with diameters on the order of 100 μm or smaller should intrude; larger droplets and gas bubbles would separate from the plume of entrained seawater and continue their ascent through the ocean water column.

The rise velocity at which a droplet (or bubble) rises in the water column, $w_s$, is known as the slip velocity, as it is the differential velocity between the vertical current velocity and the rise

velocity due to droplet (or bubble) buoyancy obtained from a drag-law correlation (Clift et al. 1978). For oil droplets up to 6–8 mm, which are spherical, the Stokes law drag correlation can accurately capture the rise velocity (Zhao et al. 2015). Larger oil droplets tend to be oblate (flattened in the horizontal direction) as they rise, and their rise velocity is commonly obtained from experimental data (Clift et al. 1978, Zheng & Yapa 2000). Individual droplets larger than 12–16 mm are unlikely to survive due to gravitational instabilities, and the maximum stable size of oil droplets is given by the Raleigh criterion (Grace 1982, Z. Li et al. 2017),

$$d_{\max} \cong 4\left[\frac{\sigma}{(\rho - \rho_o)g}\right]^{1/2}, \qquad 2.$$

where $\sigma$ is the oil–water interfacial tension, and $\rho$ and $\rho_o$ are the density of seawater and oil, respectively.

There are two broad classes of modeling approaches available to predict the dynamics of a deepwater blowout. The fundamental approach is to apply computational fluid dynamics models for the fully three-dimensional flow field, utilizing various approaches for handling the multiphase nature of the plume and a diversity of turbulence closure schemes (for a review, see Boufadel et al. 2020b). However, this approach is too computationally demanding when applied to a plume as large as the *Deepwater Horizon*'s. For this reason, the integral (or engineering-type) model approach is commonly adopted by researchers analyzing the plume-scale behavior. Integral models utilize self-similarity to derive cross-sectionally averaged equations for the plume mass, momentum, and buoyancy fluxes (Jirka 2004, Lee & Chu 2003). The governing equations are derived from conservation of mass and momentum together with an equation of state for buoyancy. The governing equations are normally closed via the entrainment hypothesis, which states that the inflow velocity of ambient water to the plume is proportional to a characteristic velocity along the plume centerline (Turner 1986). Ambient water is engulfed by turbulent eddies along the plume edges, and this entrainment results in a spreading of the plume width with distance along the plume centerline.

Before the *Deepwater Horizon* spill, several integral models for oil well blowouts included algorithms for intrusion formation and cross-flow separation based on laboratory data from Socolofsky & Adams (2002, 2005) and on results from the DeepSpill field experiment (Johansen et al. 2003). Both the Comprehensive Deepwater Oil and Gas (Chen & Yapa 2003, 2004) and DeepBlow (Johansen 2003) models are integral models based on the Lagrangian plume approach (Lee & Chu 2003). In this approach, all of the entrained ambient water flows into the first intrusion layer or the cross-flow separated plume. Above the peel or cross-flow separation height, gas bubbles or oil droplets rise as individual particles. Socolofsky et al. (2008) developed an Eulerian model that followed approaches used in lake aeration (Asaeda & Imberger 1993) to allow multiple intrusion layers to form due to stratification when there are no ambient currents. Dissanayake et al. (2018b) included each of these modeling approaches along with detailed descriptions of the separation algorithms within the Texas A&M Oilspill Calculator (TAMOC). They also summarized a broad range of validation studies, including comparisons with new experiments on oil jets in cross-flow by Murphy et al. (2016). TAMOC includes the oil equations of state from Gros et al. (2016), and Gros et al. (2017) compared the model predictions for the *Deepwater Horizon* blowout with field observations, focusing on the period around June 8, 2010.

Another mechanism that affects plume dynamics is the dissolution from gas bubbles and oil droplets; this dissolution is a complex process that is controlled by both chemistry and hydrodynamics and occurs at the bubble–water or droplet–water interface, where the saturation concentration of the bubble or droplet in equilibrium with the water is expected (Clift et al. 1978). The concentration of dissolved species then decreases with distance from the interface,

approaching the bulk water concentration outside of the chemical boundary layer surrounding a bubble or droplet. For the gas bubbles and oil droplets forming from the *Deepwater Horizon*, mass transfer, or the rate of dissolution, was limited on the seawater side by diffusion through this chemical boundary layer. Gros et al. (2017) applied the TAMOC integral plume model using an oil equation of state from Gros et al. (2016) and initial bubble and droplet size distributions from VDROP-J (Zhao et al. 2014) to predict the fate of 131 individual hydrocarbon molecules and 148 additional pseudocomponents of the *Deepwater Horizon* live oil and gas. They simulated a period near June 8, 2010, after the riser was cut and corresponding to the intensive field observations of Ryerson et al. (2011, 2012). They then predicted that all of the methane and overall 23% of the released mass flowed into the subsurface intrusion layer at 900–1,300-m depth as predominantly dissolved material, and that an additional 4% of the released mass dissolved from individual particles between the intrusion layer and the sea surface; approximately 1% of the mass was contained in small, suspended droplets. They further validated these measurements against the atmospheric data of Ryerson et al. (2011) and subsurface hydrocarbon measurements within a region up to 10 km from the release point.

Two other complicating processes at work in these simulations and in the *Deepwater Horizon* plume are worth discussing: the role of natural gas hydrates and the potential for disequilibrium of the gas–liquid partitioning of the live petroleum fluid. Natural gas hydrates are ice-like structures of gas and water that are stable at the temperatures and pressures of the *Deepwater Horizon* release. In fact, they complicated much of the response effort, including the failure of the coffer dam that was placed on the top of the wellhead to allow the capture and subsequent pumping of the oil. Warzinski et al. (2014) reported on laboratory experiments conducted at the National Energy Technology Laboratory's High-Pressure Water Tunnel Facility. Wang et al. (2016) observed similar bubbles with hydrate shells at natural gas seeps in the Gulf of Mexico. Gros et al. (2017) assumed that hydrate shells, if present, could be modeled by mass transfer coefficients for contaminated bubbles, and they therefore included this effect in their model predictions. Wang et al. (2020) further validated this assumption using data for a natural seep in the Gulf of Mexico.

The effect of gas–liquid equilibrium plays a role both in the initial conditions for the mass fractions of gas- and liquid-phase petroleum at the release and in the possible phase changes of gas bubbles or oil droplets rising through the water column. Gros et al. (2017) assumed that the gas and liquid phases of the *Deepwater Horizon* oil were at equilibrium with ambient pressure and temperature in the initial conditions of their model. They made this assumption based on the violent turbulence of the release, which would promote rapid ebullition kinetics, and on the rapid cooling of the released fluids due to the entrainment of ambient water. Pesch et al. (2018) suggested that the liquid phase may be in a supersaturated state at release or that liquid oil droplets could transition to a supersaturated state as they rise, thereby releasing a gas phase in the process of ebullition. When they conducted experiments with gas-saturated oil droplets in a counterflowing water tunnel within a pressure vessel, they observed changes in oil droplet diameter with time resulting from both dissolution and depressurization, simulating the rise of the droplet through the ocean water column. Gros et al. (2020) simulated the Pesch et al. (2018) experiments using the same model as their 2017 simulation of the *Deepwater Horizon* spill and showed the role of dissolution and the occurrence of phase transitions. Gros et al. (2017) allowed for the possibility of gas leaching from liquid droplets and vice versa by allowing each bubble or droplet to be multiphase. Gros et al.'s (2020) analysis showed that gas ebullition from live liquid oil is limited to a region close to the sea surface (i.e., in shallow waters), and in the Pesch et al. (2018) experimental apparatus, this ebullition was driven largely by the saturated gas concentration that occurred at low pressures.

To conclude the discussion of the *Deepwater Horizon* buoyant plume, we consider the important factor of subsea dispersant injection (SSDI). As explained above, bubble or droplet breakage is driven by pressure fluctuations in a turbulent flow and resisted by interfacial tension and the dispersed phase viscosity (Hinze 1955). Chemical dispersants are designed to reduce the interfacial tension, and the effect depends on the dispersant-to-oil ratio (Haza et al. 2019) and oil chemistry. Gros et al. (2017) predicted an interfacial tension reduction for the *Deepwater Horizon* oil based on laboratory experiments by Abdelrahim & Rao (2014) and on reported dispersant application rates during the period simulated (French-McCay et al. 2015). Simulations were conducted using TAMOC for initial bubble and droplet size distributions for the cases with and without SSDI. Median oil droplet sizes in the VDROP-J simulations were reduced from 4.2 mm without dispersant to 1.3 mm with dispersant. These millimeter-scale droplets were not predicted to enter the intrusion layer and surfaced within a region a few hundred meters offset from the seafloor source (Gros et al. 2017; Ryerson et al. 2011, 2012). Thus, in the sense of significantly increasing the water column sequestration of the liquid-phase petroleum, SSDI during the *Deepwater Horizon* spill was not effective. However, this shift to smaller droplets caused by SSDI dramatically increased the surface area of the oil droplets available for dissolution and slowed the rise of these smaller droplets toward the sea surface, increasing the time available for dissolution. Gros et al. (2017) predicted that, in simulations with SSDI, both of these effects would reduce the benzene emissions to the atmosphere by up to 2,000 times compared with simulations without SSDI, with reductions of a similar order of magnitude for several other soluble volatile organic chemicals. A recent study of air quality data during the *Deepwater Horizon* by Zhao et al. (2021) also showed that atmospheric emissions of volatile hydrocarbons were significantly reduced during periods of SSDI application. Thus, SSDI during the *Deepwater Horizon* spill dramatically improved the air quality in the response zone, an effect borne out by responders not being required to wear respirators when dispersants were applied subsea.

## 4. FAR-FIELD TRANSPORT PROCESSES

When not in a jet/plume, the movement of a hydrocarbon mass can be captured by the advection–diffusion equation with an additional term to account for the buoyancy of oil,

$$\frac{\partial C}{\partial t} = -(\mathbf{u} + w_s)\,\nabla C + \nabla\left(\overline{\overline{K}}\,\nabla C\right), \qquad 3.$$

where $C$ is the concentration of oil (kg/m$^3$), $\mathbf{u} = (u, v, w)$ is the water velocity, and $\overline{\overline{K}}$ is the eddy diffusivity tensor. The term concentration is used loosely herein, as a large fraction of the oil (more than 70%, depending on the oil) does not dissolve in water. The velocity (or current) is obtained from standard physical oceanography models, such as the Naval Research Laboratory's Navy Coastal Ocean Model (NCOM), which ranges from a 1-km outer nest down to a 10-m horizontal resolution (Jacobs et al. 2014) and incorporates a coupled atmosphere–wave–ocean model; the University of Miami Coupled Model (UMCM) (Chen & Curcic 2016, Curcic et al. 2016); the Hybrid Coordinate Ocean Model (HYCOM); and the Northern Gulf of Mexico (NGOM) model. These models provide the horizontal velocity in various layers, typically using sigma coordinates (i.e., following the bathymetry). The vertical velocity can be subsequently computed by integrating the continuity equation over the depth. For dissolved oil, the rise velocity is zero. Note that submicron droplets are considered to be dissolved in most environmental works, as they move with the surrounding fluid. Equation 3 or variants of it have been adopted in various works on oil transport in the Gulf of Mexico (Berenshtein et al. 2020, Bock et al. 2018, Boufadel et al. 2014, Paris et al. 2012). Equation 3 has been solved using Lagrangian techniques that are effective for domains where the relative magnitudes of advection and diffusion vary widely, which could make

the Eulerian form (i.e., Equation 3) unstable numerically (Boufadel et al. 2018a, Nordam et al. 2019).

Equation 3 does not account for forces due to droplet inertia, which are important below a size scale of 10 m and a timescale of minutes (Cui et al. 2020c, Chamecki et al. 2019). However, accounting for droplet inertia at larger scales (kilometers and hours) is computationally cost prohibitive, and actually might not be worth the effort because the uncertainty in wind, waves, and currents [including intermittent Langmuir cells (LCs) (Langmuir 1938)] has a much greater impact on droplet transport. We address first the transport due to advection (i.e., large scale).

## 4.1. Large-Scale Transport in the Gulf of Mexico

The Gulf of Mexico currents are complex and vary seasonally and on decadal scales (Oey et al. 2005) (**Figure 2**). They include the Yucatán Channel Current, which forms the Loop Current that intrudes to a variable extent into the gulf, generating energetic eddies and topographic Rossby waves (Hamilton 2009, Oey & Lee 2002), both of which propagate from east to west. In addition, currents along the northern slope pass over a bottom that is corrugated with canyons and pimpled with salt domes, which generates vertical mixing. Various works have summarized these currents (Le Hénaff et al. 2012, Welsh & Inoue 2000).

Several scientific field campaigns were conducted in the northern Gulf of Mexico following the *Deepwater Horizon* spill to better understand processes that may influence the transport of oil near the surface of the ocean, as well as to evaluate the accuracy of hydrodynamic ocean models. A variety of new instruments have been created (Özgökmen et al. 2018) to achieve unprecedented levels of dense and overlapping data sets that span large spatial and temporal scales. The

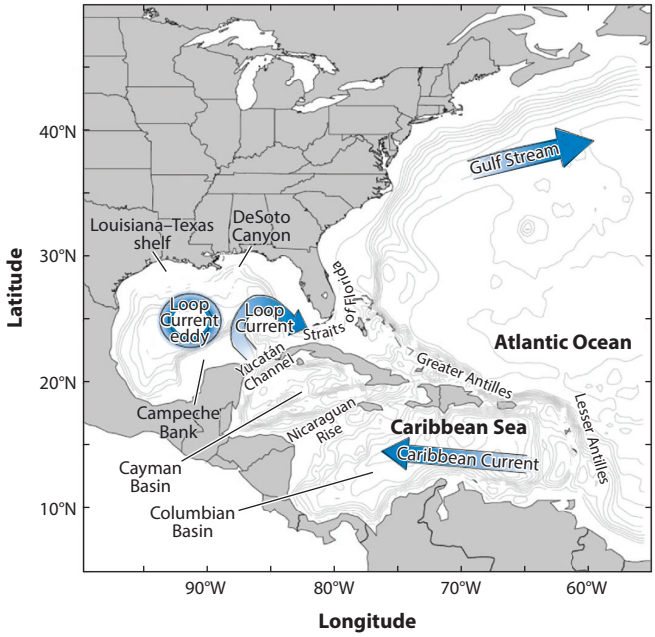


**Figure 2**

General circulation in the Gulf of Mexico and surrounding water bodies. The Yucatán Channel is a major source of high oxygen and cold water to the Gulf of Mexico. Figure adapted with permission from Oey et al. (2005).

experiments released thousands of biodegradable Lagrangian drifters, as these are naturally suited for studies of the tracer transport problem in that they do not suffer from the aliasing errors of fixed and ship-based measurements, and the researchers continued sampling the field long after the end of the cruise period, even under adverse conditions (e.g., during hurricanes; Curcic et al. 2016). **Figure 3** shows the cumulative trajectories based on the sampling of the Gulf of Mexico. After being released near the *Deepwater Horizon* region, the drifters dispersed across almost the entire basin (with the exception of continental shelves) in three to six months. A comparison with the oil concentration from the *Deepwater Horizon* event shows that undrogued Lagrangian Submesoscale Experiment (LASER) drifters have a spatial distribution that is very similar to *Deepwater Horizon* coverage, while drogued drifters followed a mesoscale filament all the way to the Mexican shelf break southward, indicating that upper-ocean vertical shear plays an important role in transport patterns. Laxague et al. (2018) presented the first-ever ocean measurements of the current vector profile defined to within 1 cm of the free surface. In these measurements, the current magnitude averaged over the upper 1 cm of the ocean was nearly four times the average over the upper 10 m.

The findings above indicate that current hydrodynamic models, which average over the upper meters of the ocean, cannot be used directly to predict the horizontal transport of oil slicks, which are usually less than 1 mm thick. One typically accounts for the movement of an oil slick on the water surface due to wind through a drift velocity that is approximately 3% of the wind speed (e.g., at 10 m) (Wu 1983). In oil spill simulation practices, the drift is allowed to vary from 1% to 6% to also capture Stokes drift (i.e., the upper limit) and because weathered oil (including oil emulsion) is heavier than fresh oil and sits lower on the water surface, resulting in less drift (ASCE Task Comm. Model. Oil Spills 1996, Boufadel et al. 2014).

Another large-scale forcing that impacted the large-scale transport of the *Deepwater Horizon* oil in the Gulf of Mexico is the Mississippi River discharge. The Mississippi River (Schwendeman et al. 2014) is the largest river in North America, with an approximate historical average discharge rate of 425 $km^3$/year (13,500 $m^3$/s) (Hu et al. 2005). Two dominant coastal flow regimes characterize the river's discharge volume into the Gulf of Mexico: a westward (downstream) current along the Louisiana–Texas shelf (west of the Mississippi) and a northeastward (upstream) current along the Mississippi–Alabama–Florida shelf (east of the Mississippi). The former is due to geostrophic balance between the Coriolis force and a cross-shelf pressure gradient (Hickey et al. 1998, Kourafalou et al. 1996, Schiller & Kourafalou 2010) and is enhanced by downwelling-favorable winds; such conditions favor material entrainment and nearshore confinement. The upstream flow is due to the balance between an along-shelf pressure gradient and along-shelf acceleration (Kourafalou et al. 1996). This upstream coastal flow has a tendency to turn offshore, enhanced in the presence of upwelling-favorable winds; such conditions promote material removal away from the coastal zone, restricting shoreward entrainment of materials from offshore sources. The third important flow regime, the buoyancy-driven anticyclonic bulge, is often suppressed due to the Mississippi Delta's proximity to a steep slope (Schiller et al. 2011, Walker et al. 1996); however, it does form under high-discharge conditions (Androulidakis & Kourafalou 2013).

The Mississippi's hydrodynamics played a significant role in the transport of hydrocarbons during the *Deepwater Horizon* incident. Kourafalou & Androulidakis (2013) used a numerical model and data-derived images of the surface oil patch (SOP) to examine the influence of Mississippi River–induced circulation on oil transport. The model was a high-resolution (1/50°, or approximately 2 km) application of HYCOM, with high-frequency forcing and detailed river plume dynamics based on work by Schiller & Kourafalou (2010). The SOP evolution was derived from the digitized maps of available observations of the surface oil slick during the *Deepwater Horizon* period, as described by Mariano et al. (2011). **Figure 4** shows examples of the synergy

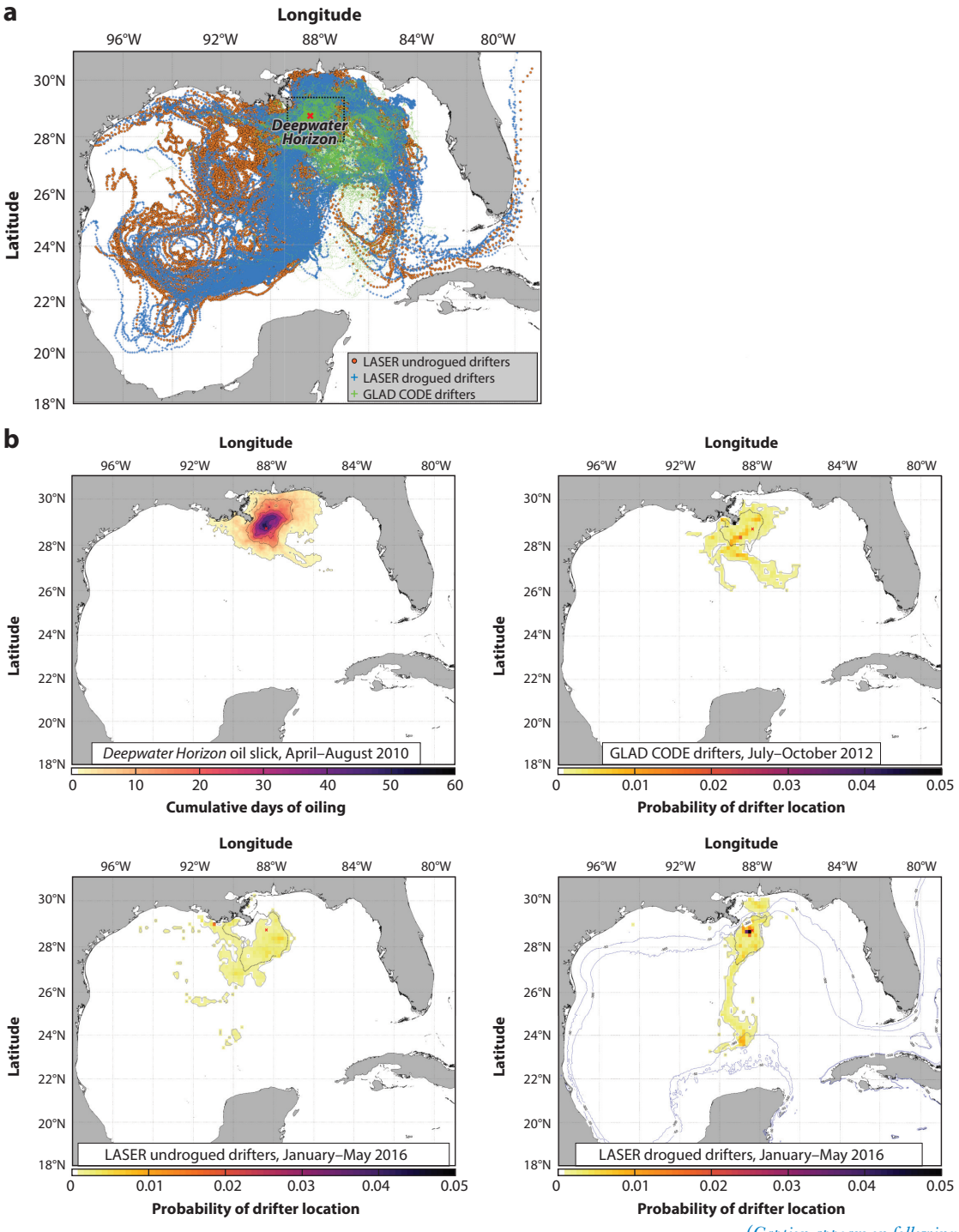


(*Caption appears on following page*)

**Figure 3** (*Figure appears on preceding page*)

(*a*) Cumulative spatial span of all CARTHE drifters deployed in the northern Gulf of Mexico. (*b*) Oil coverage from the *Deepwater Horizon* event compared with drifter density from the GLAD and LASER experiments (with LASER drogued and undrogued drifters shown separately). Abbreviations: CARTHE, Consortium for Advanced Research on Transport of Hydrocarbon in the Environment; CODE, Coastal Ocean Dynamics Experiment; GLAD, Grand Lagrangian Deployment; LASER, Lagrangian Submesoscale Experiment. Figure adapted with permission from Novelli et al. (2020).

between the offshore boundary of the model-derived Mississippi plume waters and the onshore SOP boundary. At the beginning of the *Deepwater Horizon* incident (early May 2010; **Figure 4*a***), the Mississippi discharge was at a low rate, and the winds were very light. This resulted in plume waters concentrating around the Mississippi Delta, with tendencies for limited westward (downstream) and northward (upstream) expansion. The beginning of the downstream coastal current was distinguished by a meandering plume pattern, which is characteristic of river plume development during negligible winds. The SOP had started to approach the Mississippi Delta and showed an early influence by the westward circulation due to the Mississippi plume. Toward the end of May (**Figure 4*b***), the upstream river plume circulation was well developed due to increased river discharge and downwelling-favorable winds. The SOP pattern indicates that the shoreward oil transport was inhibited by the plume, as the upstream area was dominated by offshore coastal currents. This was also evident in mid-June (**Figure 4*c***), with a clear synergy between the offshore river plume boundary and the onshore SOP boundary. The oil was prevented from moving onshore when encountering offshore river plume currents. By contrast, a strong entrainment of oil near the coast and transport toward the Louisiana–Texas shelf was observed in early July (**Figure 4*d***), under the influence of a well-established westward coastal current that resulted from strong river discharge and westward (downwelling-favorable) winds.

The buoyancy-driven downstream (westward) current was strongest during downwelling-favorable winds, when riverine waters and the SOP were advected along the Louisiana–Texas shelf (July 6; **Figure 4*d***). The upstream pathway was enhanced during upwelling-favorable winds (June 15; **Figure 4*c***). The related offshore flows within the plume front opposed the tendency for entrainment of SOP waters that characterized the downstream plume region. Consequently, the plume front formed the shoreward boundary of the SOP, keeping it away from the western Mississippi–Alabama–Florida coastal areas and the Mississippi Delta. Finally, the offshore pathways that are primarily due to the rapid removal of Mississippi River plume waters under larger-scale influences are shown in the example from May 20 (**Figure 4*b***). The related pathway has been also discussed by Schiller et al. (2011) and Walker et al. (2011) and is closely connected to the offshore spreading of the anticyclonic bulge. These findings were further quantified by data from drifters in later years (Androulidakis et al. 2018) (**Figure 5**), which showed that the drifters, whether drogued or undrogued, followed completely different trajectories depending on their locations with respect to the Mississippi's main current.

## 4.2. Submesoscale Transport

In this section we discuss salinity fronts, Langmuir circulation, and waves. Salinity fronts occur when a large freshwater mass encounters seawater. Because freshwater is less dense, it rises above the seawater, and due to the Coriolis force, the masses attempt to reach equilibrium through a rotation. Experiments using drifters in the Gulf of Mexico showed that drifters placed in a grid of $30 \times 30$ km$^2$ converged within 10 days to an area smaller than $50 \times 50$ m$^2$ (D'Asaro et al. 2018). Capturing this behavior in hydrodynamic models is not currently possible as these models cannot resolve water flow below the kilometer scale.

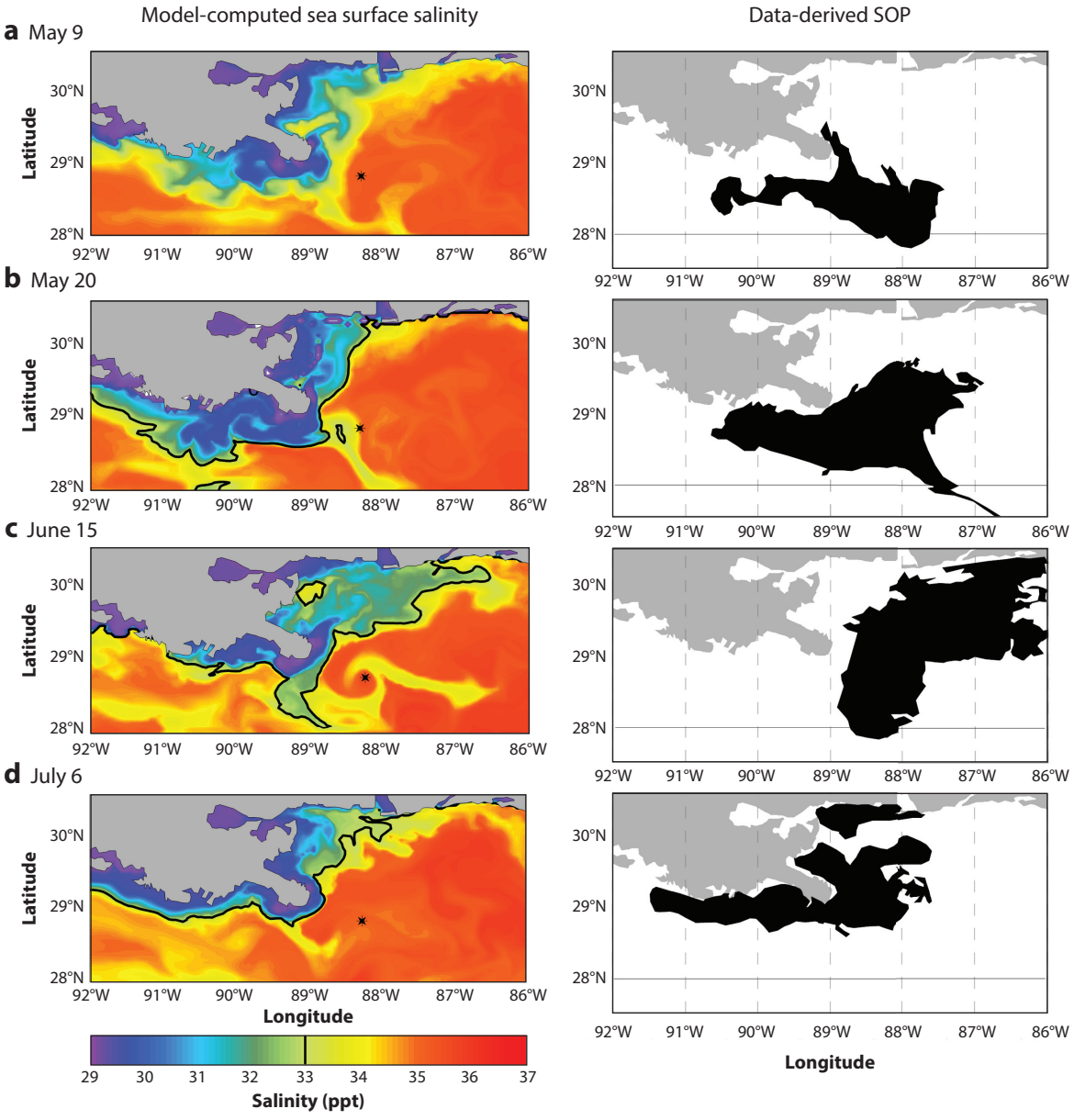


**Figure 4**

Model-computed sea surface salinity (*left*) and the data-derived SOP (*right*) (from NOAA surveys and satellite composites) (Tobin et al. 1990) on four characteristic days in 2010: (*a*) May 9, (*b*) May 20, (*c*) June 15, and (*d*) July 6. The black stars mark the location of the MC252 well. In the left-hand panels, black contours indicate a salinity of 33 ppt, which is taken to be the frontal boundary of brackish waters. In the right-hand panels, thin horizontal lines mark the southern model domain at 28°N. Abbreviations: MC252, Mississippi Canyon block 252; SOP, surface oil patch. Figure adapted with permission from Kourafalou & Androulidakis (2013).

Oil can also be transported through LCs, which form due to the interaction of wind and waves (Leibovich 1983). LCs are characterized by two counterrotating cells with a maximum downward velocity between them. The maximum upwelling velocity is usually less than half of the downwelling velocity and depends on the spacing between neighboring LCs. The strength of the LCs

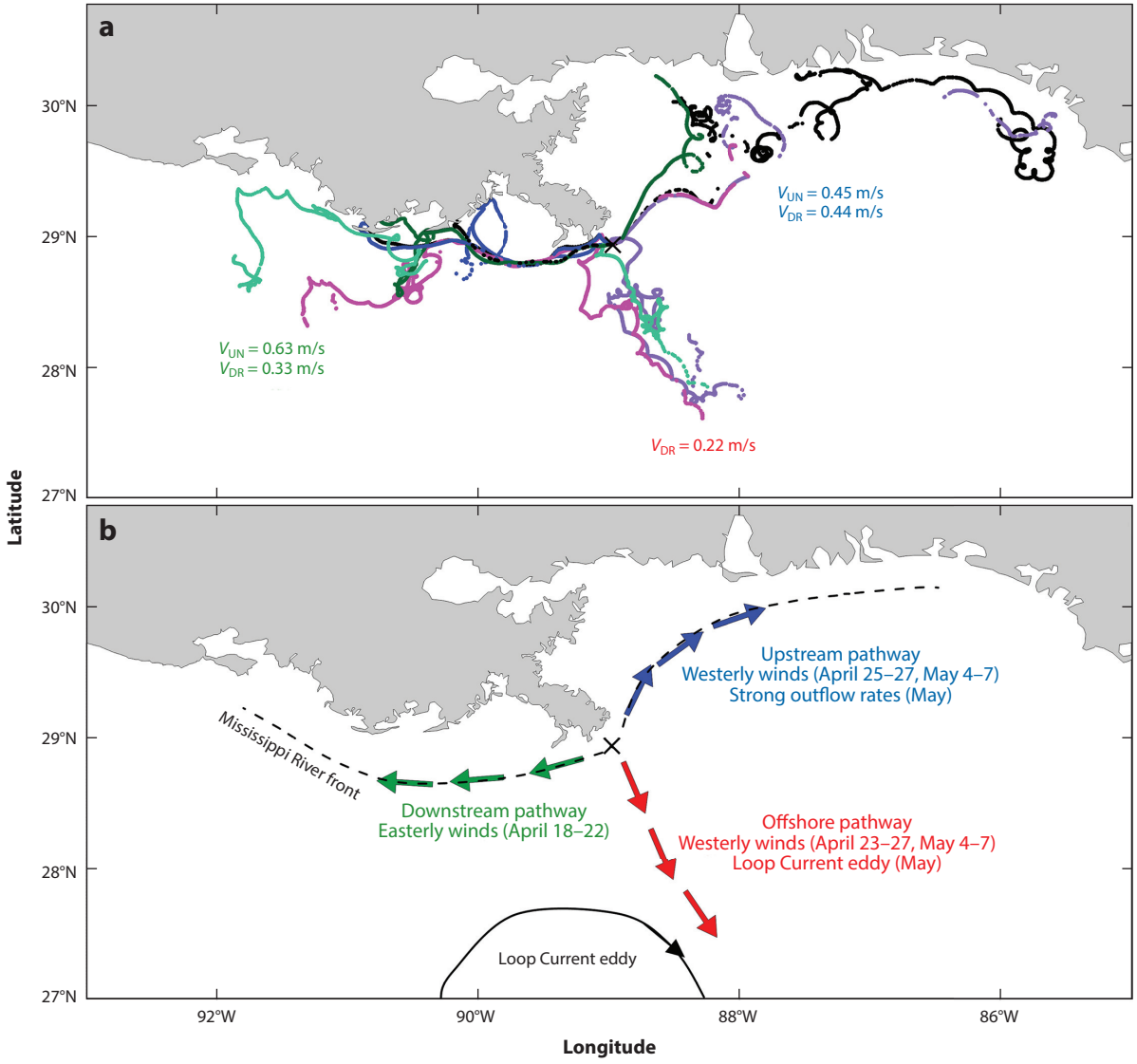


**Figure 5**

(*a*) Overall drifter trajectories from an April–June 2017 field experiment and (*b*) characteristic periods for the three potential hydrocarbon pathways (*colored arrows*: downstream, *green*; upstream, *blue*; and offshore, *red*), the Mississippi River front (*dashed line*), and the Loop Current eddy pattern (*solid line with arrow*) during the experiment period. The mean drogued ($V_{DR}$) and undrogued ($V_{UN}$) velocities and the prevailing wind directions for each pathway are also marked. Figure adapted with permission from Androulidakis et al. (2018).

may be characterized through the Langmuir number (McWilliams & Sullivan 2000):

$$La = \sqrt{\frac{u_*}{U_s}}, \qquad 4.$$

where $U_s$ is the Stokes drift at the surface, and $u_*$ is the water friction velocity given by $u_* = \sqrt{\tau_s/\rho}$ (in which $\tau_s$ is the wind shear stress on the water surface). Typical $La$ values in the ocean are

between 0.2 and 0.7. When $La \to \infty$, the LC weakens and could disappear (though Langmuir turbulence persists in the absence of the structure).

LCs can concentrate oil on the water surface in windrows (McWilliams & Sullivan 2000), which could reduce the oil–atmosphere interfacial area. The assumption of uniform horizontal oil distribution on the water surface or within a shallow depth (Vaz et al. 2021, Ward et al. 2018) could potentially lead to overestimates of the extent of photooxidation and/or evaporation, as both of these processes increase with the oil–atmosphere surface area. Farmer & Li (1994) used a hypothetical stream function formulation for a cross section of an LC (i.e., perpendicular to the wind direction) to obtain the water velocity distribution in an LC. They showed that the LC would enhance the vertical diffusion of small droplets, but large droplets (millimeter sized) have a large buoyancy velocity that balances the downwelling water velocity, leading to the formation of Stommel retention zones, whereby the oil is trapped. Stommel cells of air bubbles have been reported in LCs (Thorpe 1984). Yang et al. (2014) considered the situation where the wind is exactly aligned with waves and found that LCs inhibit the spreading of floating matter. Noting that the downwelling velocity scales with the Stokes drift (due to waves), they introduced a dimensionless number, $D_b = U_s/w_s$, to consider situations where the LC enhances or inhibits the vertical diffusion of oil droplets. They also classified the oil slick on the water surface as fingered, blurred, or diluted and related these classifications to $D_b$ and $La$ using large-eddy simulations.

The investigations at the LC scale provided important physical insights into transport within an LC, but challenges remain to scale up such results. First, the cells have life spans from minutes to tens of minutes and break and merge together in Y-shaped configurations. In addition, the depth of the cells could reach the mixed-layer depth, but the cells could also dissolve before that occurs. Also, in the general situation of the wind not being exactly aligned with the direction of wind propagation, the oil crosses LCs, and thus, the presence of LCs enhances the horizontal dispersion (diffusion) of oil rather than restricting transport, as is found when the air is exactly aligned with the LC (Yang et al. 2014).

Simecek-Beatty & Lehr (2017) provided a framework to account for the reduction of the surface area of slicks due to LCs; they used equations from the literature for the spacing between the LCs as a function of the wind speed and assumed that the oil thickness is uniform in the convergence zones. They also captured the facts that the number of LCs containing oil decreases with time (as old LCs containing oil disappear and new clean ones emerge) and that the length of oiled cells increases with time. Thus, the net role of Langmuir circulation is to enhance the vertical and horizontal dispersion of oil and could potentially reduce its photooxidation and evaporation.

Ekman transport (Ekman 1905) is due to the interaction of the Coriolis force with horizontal velocities generated by wind. From a theoretical point of view, it causes particles at the surface to move at 45° with the wind direction, and the magnitude of that transport decreases with the latitude. However, Lodise et al. (2019) found that, due to a variety of factors (waves, LCs, and transient local wind directions), the angle in the Gulf of Mexico varies from 0° to more than 90°. Therefore, it is not possible to simulate the transport due to Ekman transport when dealing with transport at scales much smaller than the mesoscale.

The kinematics of waves are well captured using potential flow theories (Dean & Dalrymple 1991), the simplest of which is the linear wave theory, also known as the first-order theory. The Stokes theory is most relevant to the transport of matter, because it results in a net forward drift of matter within the wave, which is due to the asymmetric nature of an ocean wave (approximated by the Stokes wave). The waves at sea are irregular (different wave periods and heights) and thus are described using a wave spectrum (Bretschneider 1959, Phillips 1958). A widely used spectrum is the Joint North Sea Wave Project (JONSWAP) spectrum (Hasselmann et al. 1973). It has been common to integrate the one-dimensional spectrum over the frequency to obtain the cumulative

Stokes drift. This approach, however, tends to overestimate the drift, and a more accurate approach is to also integrate over the directions (Webb & Fox-Kemper 2015).

Elliott (1986) released oil and dye in a 45-m-deep estuary in the North Sea and concluded that shear dispersion due to the Stokes profile played an important role in the horizontal spreading of oil. They assumed that that the vertical transport was due to a constant vertical eddy diffusivity of $10^{-3}$ $m^2/s$. They explained the comet shape of the oil—where the highest concentration is in the front, followed by a tail of low concentrations—as resulting from Stokes drift and buoyancy; large droplets stay closer to the water surface, where the Stokes drift is largest. Boufadel et al. (2006, 2007) numerically investigated the transport of oil droplets within regular waves using the Stokes theory and captured the transport of oil droplets between the mean water level and the crest using a Taylor expansion. They also assumed that the local turbulent coefficient decreases with depth, following the expression of Ichiye (1967). Geng et al. (2016) expanded this work to irregular waves that are represented by a JONSWAP spectrum and estimated horizontal and diffusion coefficients. These works found that the horizontal diffusion coefficient increases with the wave height and that oil transport models that address only the transport of oil slicks on the water underestimate the horizontal diffusion coefficient.

In experiments in wave tanks where wave breakers were generated, Delvigne & Sweeney (1988) found that the number of oil droplets of size (diameter) $d$ in water, $N(d)$, is given by

$$N(d) \sim d^{-a}, \qquad 5.$$

where $a$ is approximately 2.1–2.3. Equation 5 indicates that the number of droplets in the water column following breaking decreases with the diameter size, which is intuitive, as larger droplets are entrained less due to their buoyancy. Experiments with solitary breakers in a wave tank by the Katz group at Johns Hopkins (C. Li et al. 2017) reported that after 10 min, Equation 5 was applicable for droplets smaller than 1 mm, and the slope increased rapidly (with $a$ reaching a value of 9) for droplets larger than 1 mm (meaning that there are fewer of them in the water column). The Boufadel team (Cui et al. 2020b) noted the same result in oil dispersion studies conducted in Fisheries and Oceans Canada's wave tank at the Bedford Institute of Technology. They also noted that the volume-based droplet size distribution is Gaussian and thus would lead to Equation 5 for droplets smaller than the volume mean diameter, which was approximately 1.0 mm.

Wave breaking both tears the oil slick and entrains oil into the water column, and expressions for entrainment of oil droplets into the water column have been developed (Delvigne & Sweeney 1988; Mackay et al. 1980, 1986). The concept of entrainment of oil droplets into the water column due to breaking then became the cornerstone of earlier oil spill models, probably because at the time the focus was on the transport of oil on the water surface, and thus there was a need for a mechanism for removing oil from the water surface. In addition, the entrainment expressions were developed in wave tanks and therefore do not account for the background turbulence present at sea. Liu et al. (2022) proposed an alternative approach in which they considered wave breaking to be due to whitecaps (i.e., a direct action by wind) and thus to not extend too deep into the water column. The subsequent vertical transport of droplets was assumed to be due to droplet buoyancy and turbulent diffusion. Liu et al. (2022) found that a steady-state profile of droplets is reached within minutes. They also noted that the values for the energy dissipation rate adopted in hydrodynamic models (Craig & Banner 1994, Large et al. 1994) are too small (approximately $10^{-4}$ W/kg) to generate oil droplets from a slick, as the latter mechanism requires energy dissipation rates on the order of $10^{-2}$ W/kg or higher (Cui et al. 2020a,c; C. Li et al. 2017). This is due to the fact that the energy dissipation rates used in hydrodynamic models are averaged over space and time, as their purpose is to balance the average shear stress due to wind, and thus they could not reproduce the instantaneous increase in energy dissipation rate during wave breaking.

## 4.3. Eddy Diffusivity

A diffusion formulation is commonly adopted to parameterize transport of matter (solutes and oil) occurring below the resolved temporal and/or spatial scale. Therefore, with the exception of molecular diffusion, which depends on the energy level of atoms (Einstein 1905), the term diffusion coefficient (or diffusivity) depends on the hydrodynamics and scales of the system (Boland et al. 2015). The value of the eddy diffusivity has direct implications for the dilution and mixing of oil in the water column, which impacts hydrocarbon dissolution and biodegradation (Prince et al. 2013, Valentine et al. 2010) and toxicity (Bejarano et al. 2014, 2016).

It is well established that the horizontal eddy diffusivity follows Richardson's law of diffusion in turbulent flows, $K_h \sim \ell^{4/3}$, where $\ell$ is the length of the plume (Richardson 1926)—a law confirmed with oceanic field data from Okubo (1971) and various recent works. For example, by using satellite data from multiple years, Nummelin et al. (2021) found that the horizontal diffusivity reaches up to $10^4$ m$^2$/s at the 1,000-km scale. However, unlike the transport of salt water masses, the modeling of oil spills requires submesoscale (i.e., less than 10 km in the horizontal) resolution due to the hazardous nature of oil and the sizes of the plumes (less than tens of kilometers). At the submesoscale or below, the horizontal eddy diffusivity is less than $10^2$ m$^2$/s and is due to vortical modes, fronts, Langmuir turbulence, and waves (Davis 1985). We address here how these studies compare with Richardson's four-thirds law.

Three complementary studies were made possible by the accidental loss of the drogues from 40% of the LASER drifters because of the strong El Niño winds and waves; these undrogued drifters were subsequently distinguished from the ones that still had their drogues, creating two data sets that sampled the ocean at two different depths (Haza et al. 2018). Haza et al. (2019) used this information to develop wind- and wave-based models to supplement the upper-ocean transport capability of NCOM, leading to a significant increase in skill. Lodise et al. (2019) employed the same data set to discern wind, wave, and ocean current effects in the upper 1 m of the ocean. Novelli et al. (2020) compiled the results from the entire Consortium for Advanced Research on Transport of Hydrocarbon in the Environment (CARTHE) drifter data set and found that undrogued drifters, which experienced Stokes drift more than the drogued ones (per laboratory and field testing in Novelli et al. 2017), were substantially more likely to reach the shorelines than the drogued drifters and generally landed in the same places where oil was found following the *Deepwater Horizon* event. This finding emphasizes the importance of wave drift regarding landfall, as landfall is arguably the most socioeconomically damaging aspect of oil spills.

The striking new finding is that, while the field results are consistent with $K_h \sim \ell^{4/3}$, there is a jump in diffusivity by almost an order of magnitude at scales below 1,000 m (**Figure 6*a***), which is where submesoscales start kicking in, as well as under hurricane conditions (**Figure 6*b***). Chang et al. (2019) pointed out that another interesting deviation from Richardson's four-thirds law occurs because of the anisotropy in Langmuir turbulence embedded in the near-surface circulation.

Studies have additionally found that upper-ocean shear and wave effects were also pronounced under low-wind conditions. In this regime, it is hard to differentiate contributions from convection and Langmuir turbulence (Mensa et al. 2015, Wang & Özgökmen 2018) or possibly other processes (see figure 3 in Özgökmen et al. 2016).

In contrast to the horizontal or isopycnal diffusivity, which increases with scale, the vertical eddy diffusivity, $K_v$, has a distinct profile in the mixed layer and then decreases to a value of $10^{-5}$ m$^2$/s in the ocean interior (Ledwell et al. 2011) before increasing rapidly to $10^{-4}$ m$^2$/s near the bottom due to shear as a result of currents interacting with the bottom (Ledwell et al. 2016). Bracco et al. (2020) elucidated how a sloped and rough bottom boundary can be a major mechanism for engendering shear dispersion and enhancing mixing.

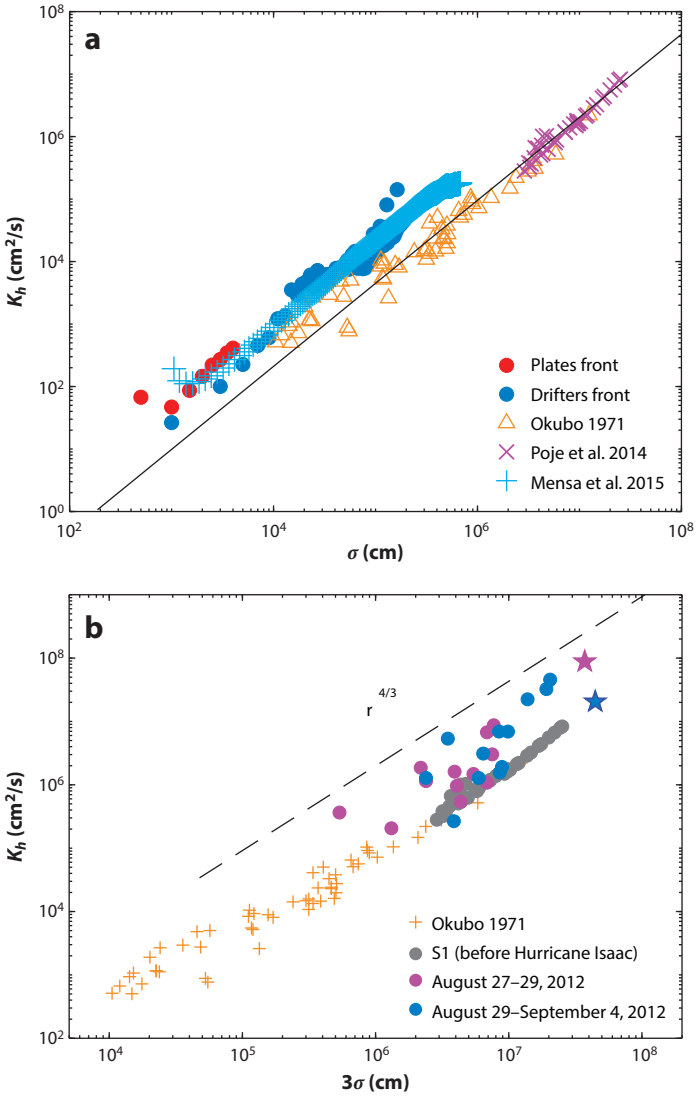


**Figure 6**

Scale-dependent diffusivities from CARTHE expeditions under (*a*) normal forcing and (*b*) hurricane forcing. In panel *b*, S1 refers to the S1 GLAD deployment. Abbreviations: CARTHE, Consortium for Advanced Research on Transport of Hydrocarbon in the Environment; GLAD, Grand Lagrangian Deployment. Panel *a* adapted from Carlson et al. (2018) (CC BY 4.0); panel *b* adapted with permission from Curcic et al. (2016).

The eddy diffusivity in the upper ocean deserves particular attention due to oil buoyancy. Although turbulent diffusion occurs both upward and downward, the water surface constitutes an upper boundary for buoyant matter, and thus diffusion is the only mechanism that brings such matter into the water column. If the vertical eddy diffusivity, $K_v$, is modeled as uniform, then the concentration of droplets with the rise velocity, $w_s$, at the water surface satisfies (Boufadel et al. 2020a)

$$c(z = 0, t \to \infty) \sim \frac{w_s}{K_v}. \qquad 6.$$

That is, as time moves forward, the concentration at the water surface of an oil droplet of a given size increases with its rise velocity and decreases with the eddy diffusivity. This also means that neutrally buoyant particles ($w_s = 0$) will ultimately diffuse downward from the water surface.

The adoption of a vertically uniform eddy diffusivity in the mixed layer is a convenience, as the value there is much larger than the eddy diffusivity in the ocean's interior (Berenshtein et al. 2020, Paris et al. 2012). Recent works related to the transport of oil droplets (Boufadel et al. 2018a, 2020a; Nordam et al. 2019) have pointed out the commonly known fact in physical oceanography that the eddy diffusivity varies with depth within the mixed layer, reaching a maximum in the upper third of the mixed-layer depth. Craig & Banner (1994) and Large et al. (1994) presented seminal work on this topic, and various parameterizations are currently available on the General Ocean Turbulence Model website (**http://gotm.net**). The formulation of Craig & Banner (1994) generates a sharp (bilinear) profile of $K$ and thus is not very amenable to numerical simulations. Visser (1997) proposed an empirical expression of $K$ as $K = az\exp(-bz)$, where $a$ and $b$ are empirical constants. The formulation proposed by Large et al. (1994) is the so-called the K-Profile Parameterization (KPP) model and provides a smooth, gradually varying profile:

$$K_v = \left(\frac{\kappa u_*}{\phi}\theta\right) z\left(1 - \frac{z}{MLD}\right)^2, \tag{7.}$$

where $u_*$ is the water friction velocity; $\phi$ is the stability function in the Monin–Obukov theory for boundary layers (Monin & Yalgom 1975), approximately 0.9; and $MLD$ is the mixed-layer depth. At greater depths, one reaches the interior of the ocean, which is dominated by stratification. The term $\theta$ is an enhancement factor that depends inversely on the Langmuir number $La = \sqrt{u_*/U_s}$. When $La \to \infty$, the LC is negligible to nonexistent, which leads to $\theta \to 1$. Conversely, as $La$ tends to zero (i.e., the LC becomes stronger), $\theta$ increases (exceeding 1.0), reflecting the fact that LCs enhance the vertical diffusion of matter in the mixed layer.

The value of $K_v$ at the water surface based on the KPP formulation is $K_v\,(0) = 0$, and thus oil droplets at the water surface can never move downward by turbulent diffusion, which is not realistic. However, based on the boundary-layer theory, as one approaches the boundary, surface roughness plays a role, and thus $z$ in Equation 8 reaches a constant value equal to the roughness scale of turbulence, $z_0$ (Townsend 1980). The value of $z_0$ could represent the surface roughness due to regular waves (i.e., comparable to the wave height) or could represent a wave-enhanced layer, as posited by Craig & Banner (1994). Based on these arguments, Boufadel et al. (2020a) adopted the following form:

$$K_v = \left(\frac{\kappa u_*}{\phi}\theta\right) (z + z_0)\left(1 - \frac{z}{MLD}\right)^2. \tag{8.}$$

In Equation 8, when $z = 0$, $K_v$ takes the value

$$K_v(z = 0) = \left(\frac{\kappa u_*}{\phi}\theta\right) z_0, \tag{9.}$$

a nonzero value allowing downward transport of materials from the water surface. Nevertheless, it is worth noting that models for the vertical eddy diffusivity assume steady-state hydrodynamics, which could be violated if the timescale of interest is short (e.g., hours or days), as is typical when dealing with oil spills, where authorities responding to the spill must make daily decisions (MacFadyen et al. 2011).

## 5. FORMATION OF OIL–PARTICLE AGGREGATES ON SHORELINES

As oil approaches shorelines, it interacts with sediments and forms so-called oil–particle aggregates (Fitzpatrick et al. 2015; Johnson et al. 2018; Lee et al. 2015; Zhao et al. 2016, 2017a). These

aggregates have different names depending on their size, shape, and composition (Boglaienko & Tansel 2018, Gustitus & Clement 2017, Hayworth et al. 2011) and on the need to communicate these properties to responders. In terms of the oil spill response by the US government, the technique for locating, characterizing, and describing oil on the shorelines is known as the shoreline cleanup and assessment technique (SCAT) (Hayes & Michel 1998, Michel & Hayes 1993, Michel et al. 2013, Owens & Sergy 2000, Taylor & Reimer 2008).

For the *Deepwater Horizon* spill, the oil that reached the shorelines was heavily weathered and therefore had a relatively high density (comparable to that of freshwater) and a large viscosity. The latter plays a major factor in keeping the oil slick together and thus is the precursor for the formation of submerged oil mats (SOMs), whose dimensions are meters in the cross-shore direction, meters to tens of meters in the alongshore direction, and centimeters in thickness. SOMs are considered primary deposits in the sense that the oil that formed them came directly from offshore. They formed either because the oil slick accumulated enough sediments to cause it to sink or because the slick became stranded onshore behind a falling tide. Plant et al. (2012) used a depth-averaged hydrodynamic model to describe the transport of sediments and oil in the shore zone with forcing from the HYCOM model and a JONSWAP spectrum. Based in part on the modeling results, the Operational Science Advisory Team concluded that the SOMs mostly formed landward of the first sand bar because the concentration of sediment that could reach the surface seaward of the sand bar is small and thus too low to alter the density of the slick and cause it to sink (OSAT-3 2013). This seems plausible for the majority of the SOMs, when the oil slick is moving cross-shore to the surf zone. However, one might need to also consider situations where the residence time of the slick in the shore zone seaward of the sand bar is on the order of tens of minutes, a timescale at which sufficient sediment particles would have attached to it, as observed in laboratory studies (Ji et al. 2021a,b). The situation of a long residence time of oil would occur, for example, at the exits of jetties or passes or at night due to land breeze (blowing seaward). Some groups have surmised that LCs could also form in shallow zones during storms and bring up the sediments to the surface, which would enhance the formation of oil–particle aggregates (Smith et al. 2019). However, it is difficult to demonstrate that SOMs form seaward of the sand bar due to the lack of visibility at large depths. In fact, most of the SOMs reported in the Gulf of Mexico were based on the so-called snorkel-SCAT method (OSAT-3 2013), which covers depths less than a few meters.

Other categories of oil–particle aggregates include patties, which can range in diameter from 10 to 100 cm and can be primary or secondary deposits, the latter of which implies that they are the result of fragmentation of SOMs. Primary patty deposits are commonly found in low-energy environments, such as the back sides of barrier islands, but a small percentage of them have been found in beaches facing the Gulf of Mexico. Another category is surface residue balls (SRBs), which have diameters of a few centimeters; in spite of their name, SRBs are ellipsoid or even irregular in shape, rather than spherical (Gustitus & Clement 2017). They are generally the result of a secondary deposit caused by the fragmentation of SOMs and are usually found in the intertidal zone, although some occur in the subtidal zone. Unlike SOMs and patties, which contain considerable amounts of oil (upward of 80% per volume), SRBs are made up of 80–96% sand, with oil constituting the rest, and the oil is highly weathered (OSAT-2 2011). The mechanism for deposition of SRBs results from a deceleration of the horizontal flow because of either horizontal divergence or convergence of the longshore currents. Plant et al. (2012) found that the mobility of sand determined, to a large extent, the mobility of the SRBs, but there was no direct relation to the net displacement of the SRBs, as the motion could be periodic; they also found that SRBs reaching the shore during normal conditions must have come from regions immediately offshore, as longshore currents could not displace SRBs except during storm events. The investigations of

oil–particle aggregates revealed that, despite the availability of sophisticated models for sediment transport in the shore zone, modeling the transport of these aggregates there remains challenging due to their irregular shapes and relatively low concentrations, which make it difficult to identify general laws about their transport.

## 6. CONCLUSIONS

The uncertainty in understanding the transport and behavior of the *Deepwater Horizon* spill stems from the large depth that it emanated from (1.5 km), the formation of oil droplets at the wellhead and in wind waves, the complex flows in the Gulf of Mexico, and the interaction of oil with sediment as the oil entered the shore zone. This review has aimed to address the role of physical oceanography in the transport of this oil. Jet/plume dynamics played a major role in the subsequent transport of the oil due to the formation of an intrusion layer at 1,300 m and the formation of oil droplets of various size. A limitation of existing hydrodynamic models was the lack of data at depth to calibrate these models. Models of oil transport in the mixed layer and of the water surface are generally reliable within a few kilometers in the horizontal direction, but the accuracy decreases near the Mississippi River due to the presence of fronts. Capturing the vertical transport of oil in the mixed layer remains a challenge due to the sharp variation of the horizontal velocity with depth and due to wave breaking. Recent field studies in the Gulf of Mexico indicate that the horizontal eddy diffusivity exceeds the four-thirds law below the submesoscale. Our goal was to present critical findings and developments in oil transport in each compartment in the Gulf of Mexico and to present the results in a way that enhances communication among scientists, engineers, and various other entities, including the government, industry, and academia.

## DISCLOSURE STATEMENT

The authors are not aware of any affiliations, memberships, funding, or financial holdings that might be perceived as affecting the objectivity of this review.

## ACKNOWLEDGMENTS

This work was made possible by the Oceans Protection Plan from Fisheries and Oceans Canada through the Multi-Partner Research Initiative and by the Gulf of Mexico Research Initiative through CARTHE (**http://carthe.org**). However, no official endorsement of the work by these entities is implied.

## LITERATURE CITED

Abdelrahim M, Rao DN. 2014. Measurement of interfacial tension in hydrocarbon/water/dispersant systems at deepwater conditions. In *Oil Spill Remediation: Colloid Chemistry-Based Principles and Solutions*, ed. P Somasundaran, P Patra, RS Farinato, K Papadopoulos, pp. 295–315. New York: Wiley & Sons

Aeppli C, Carmichael CA, Nelson RK, Lemkau KL, Graham WM, et al. 2012. Oil weathering after the *Deepwater Horizon* disaster led to the formation of oxygenated residues. *Environ. Sci. Technol.* 46:8799–807

Androulidakis YS, Kourafalou VH. 2013. On the processes that influence the transport and fate of Mississippi waters under flooding outflow conditions. *Ocean Dyn.* 63:143–64

Androulidakis YS, Kourafalou VH, Özgökmen T, Garcia-Pineda O, Lund B, et al. 2018. Influence of river-induced fronts on hydrocarbon transport: a multiplatform observational study. *J. Geophys. Res. Oceans* 123:3259–85

Asaeda T, Imberger J. 1993. Structure of bubble plumes in linearly stratified environments. *J. Fluid Mech.* 249:35–57

ASCE Task Comm. Model. Oil Spills. 1996. State-of-the-art review of modeling transport and fate of oil spills. *J. Hydraul. Eng.* 122:594–609

Baldyga J, Podgórska W. 1998. Drop break-up in intermittent turbulence: maximum stable and transient sizes of drops. *Can. J. Chem. Eng.* 76:456–70

Bejarano AC, Clark JR, Coelho GM. 2014. Issues and challenges with oil toxicity data and implications for their use in decision making: a quantitative review. *Environ. Toxicol. Chem.* 33:732–42

Bejarano AC, Farr JK, Jenne P, Chu V, Hielscher A. 2016. The Chemical Aquatic Fate and Effects database (CAFE), a tool that supports assessments of chemical spills in aquatic environments. *Environ. Toxicol. Chem.* 35:1576–86

Berenshtein I, Paris CB, Perlin N, Alloy MM, Joye SB, Murawski S. 2020. Invisible oil beyond the *Deepwater Horizon* satellite footprint. *Sci. Adv.* 6:eaaw8863

Bock M, Robinson H, Wenning R, French-McCay D, Rowe J, Walker AH. 2018. Comparative risk assessment of oil spill response options for a deepwater oil well blowout: part II. Relative risk methodology. *Mar. Pollut. Bull.* 133:984–1000

Boglaienko D, Tansel B. 2018. Classification of oil–particle interactions in aqueous environments: aggregate types depending on state of oil and particle characteristics. *Mar. Pollut. Bull.* 133:693–700

Boland EJ, Shuckburgh E, Haynes PH, Ledwell JR, Messias M-J, Watson AJ. 2015. Estimating a submesoscale diffusivity using a roughness measure applied to a tracer release experiment in the southern ocean. *J. Phys. Oceanogr.* 45:1610–31

Boufadel MC, Abdollahi-Nasab A, Geng X, Galt J, Torlapati J. 2014. Simulation of the landfall of the Deepwater Horizon oil on the shorelines of the Gulf of Mexico. *Environ. Sci. Technol.* 48:9496–505

Boufadel MC, Bechtel RD, Weaver J. 2006. The movement of oil under non-breaking waves. *Mar. Pollut. Bull.* 52:1056–65

Boufadel MC, Cui F, Katz J, Nedwed T, Lee K. 2018a. On the transport and modeling of dispersed oil under ice. *Mar. Pollut. Bull.* 135:569–80

Boufadel MC, Du K, Kaku VJ, Weaver JW. 2007. Lagrangian simulation of oil droplets transport due to regular waves. *Environ. Model. Softw.* 22:978–86

Boufadel MC, Gao F, Zhao L, Özgökmen T, Miller R, et al. 2018b. Was the Deepwater Horizon well discharge churn flow? Implications on the estimation of the oil discharge and droplet size distribution. *Geophys. Res. Lett.* 45:2396–403

Boufadel MC, Liu R, Zhao L, Lu Y, Özgökmen T, et al. 2020a. Transport of oil droplets in the upper ocean: impact of the eddy diffusivity. *J. Geophys. Res. Oceans* 125:e2019JC015727

Boufadel MC, Socolofsky SA, Katz J, Yang D, Daskiran C, Dewar W. 2020b. A review on multiphase underwater jets and plumes: droplets, hydrodynamics, and chemistry. *Rev. Geophys.* 58:e2020RG000703

Bracco A, Paris CB, Esbaugh AJ, Frasier K, Joye S, et al. 2020. Transport, fate and impacts of the deep plume of petroleum hydrocarbons formed during the Macondo blowout. *Front. Mar. Sci.* 7:764

Bretschneider CL. 1959. *Wave variability and wave spectra for wind-generated gravity waves*. Tech. Memo. 118, US Army Corps Eng., Washington, DC

Calabrese RV, Chang TPK, Dang PT. 1986. Drop breakup in turbulent stirred-tank contactors. Part I: effect of dispersed-phase viscosity. *AIChE J.* 32:657–66

Carlson DF, Özgökmen T, Novelli G, Guigand C, Chang H, et al. 2018. Surface ocean dispersion observations from the ship-tethered aerostat remote sensing system. *Front. Mar. Sci.* 5:479

Chamecki M, Chor T, Yang D, Meneveau C. 2019. Material transport in the ocean mixed layer: recent developments enabled by large eddy simulations. *Rev. Geophys.* 57:1338–71

Chang H, Huntley HS, Kirwan AD Jr., Carlson DF, Mensa JA, et al. 2019. Small-scale dispersion in the presence of Langmuir circulation. *J. Phys. Oceanogr.* 49:3069–85

Chen F, Yapa PD. 2003. A model for simulating deep water oil and gas blowouts—part II: comparison of numerical simulations with "Deepspill" field experiments. *J. Hydraul. Res.* 41:353–65

Chen F, Yapa PD. 2004. Modeling gas separation from a bent deepwater oil and gas jet/plume. *J. Mar. Syst.* 45:189–203

Chen SS, Curcic M. 2016. Ocean surface waves in Hurricane Ike 2008 and Superstorm Sandy 2012: coupled model predictions and observations. *Ocean Model.* 103:161–76

Clift R, Grace JR, Weber ME. 1978. *Bubbles, Drops, and Particles*. New York: Academic
Craig PD, Banner ML. 1994. Modeling wave enhanced turbulence in the ocean surface layer. *J. Phys. Oceanogr.* 24:2546–59
Cui F, Daskiran C, King T, Robinson B, Lee K, et al. 2020a. Modeling oil dispersion under breaking waves. Part I: wave hydrodynamics. *Environ. Fluid Mech.* 20:1527–51
Cui F, Geng X, Robinson B, King T, Lee K, Boufadel MC. 2020b. Oil droplet dispersion under a deep-water plunging breaker: experimental measurement and numerical modeling. *J. Mar. Sci. Eng.* 8:230
Cui F, Zhao L, Daskiran C, King T, Lee K, et al. 2020c. Modeling oil dispersion under breaking waves. Part II: coupling Lagrangian particle tracking with population balance model. *Environ. Fluid Mech.* 20:1553–78
Curcic M, Chen SS, Özgökmen TM. 2016. Hurricane-induced ocean waves and stokes drift and their impacts on surface transport and dispersion in the Gulf of Mexico. *Geophys. Res. Lett.* 43:2773–81
D'Asaro EA, Shcherbina AY, Klymak JM, Molemaker J, Novelli G, et al. 2018. Ocean convergence and the dispersion of flotsam. *PNAS* 115:1162–67
Davis RE. 1985. Drifter observations of coastal surface currents during CODE: the method and descriptive view. *J. Geophys. Res. Oceans* 90:4741–55
Dean RG, Dalrymple RA. 1991. *Water Wave Mechanics for Engineers and Scientists*. Singapore: World Sci.
Delvigne GA, Sweeney C. 1988. Natural dispersion of oil. *Oil Chem. Pollut.* 4:281–310
Dissanayake AL, Burd AB, Daly KL, Francis S, Passow U. 2018a. Numerical modeling of the interactions of oil, marine snow, and riverine sediments in the ocean. *J. Geophys. Res. Oceans* 123:5388–405
Dissanayake AL, Gros J, Socolofsky SA. 2018b. Integral models for bubble, droplet, and multiphase plume dynamics in stratification and crossflow. *Environ. Fluid Mech.* 18:1167–202
Einstein A. 1905. On the electrodynamics of moving bodies. *Ann. Phys.* 17:891–921
Ekman VW. 1905. On the influence of the earth's rotation on ocean-currents. *Ark. Mat. Astron. Fys.* 2(11):1–52
Elliott AJ. 1986. Shear diffusion and the spread of oil in the surface layers of the North Sea. *Dtsch. Hydrogr. Z.* 39:113–37
Farmer D, Li M. 1994. Oil dispersion by turbulence and coherent circulations. *Ocean Eng.* 21:575–86
Fay JA. 1969. The spread of oil slicks on a calm sea. In *Oil on the Sea*, ed. DP Hoult, pp. 53–63. Boston: Springer
Fitzpatrick FA, Boufadel MC, Johnson R, Lee K, Graan TP, et al. 2015. *Oil-particle interactions and submergence from crude oil spills in marine and freshwater environments: review of the science and future research needs*. Open-File Rep. 2015-1076, US Geol. Surv., Reston, VA
French-McCay DP, Jayko K, Li Z, Horn M, Kim Y, et al. 2015. *Technical reports for Deepwater Horizon water column injury assessment: WC_TR14: modeling oil fate and exposure concentrations in the deepwater plume and cone of rising oil resulting from the Deepwater Horizon oil spill*. Rep., RPS ASA, South Kingstown, RI
Geng X, Boufadel MC, Özgökmen T, King T, Lee K, et al. 2016. Oil droplets transport due to irregular waves: development of large-scale spreading coefficients. *Mar. Pollut. Bull.* 104:279–89
Grace HP. 1982. Dispersion phenomena in high viscosity immiscible fluid systems and application of static mixers as dispersion devices in such systems. *Chem. Eng. Commun.* 14:225–77
Gros J, Arey JS, Socolofsky SA, Dissanayake AL. 2020. Dynamics of live oil droplets and natural gas bubbles in deep water. *Environ. Sci. Technol.* 54:11865–75
Gros J, Reddy CM, Nelson RK, Socolofsky SA, Arey JS. 2016. Simulating gas–liquid–water partitioning and fluid properties of petroleum under pressure: implications for deep-sea blowouts. *Environ. Sci. Technol.* 50:7397–408
Gros J, Socolofsky SA, Dissanayake AL, Jun I, Zhao L, et al. 2017. Petroleum dynamics in the sea and influence of subsea dispersant injection during *Deepwater Horizon*. *PNAS* 114:10065–70
Gustitus SA, Clement TP. 2017. Formation, fate, and impacts of microscopic and macroscopic oil-sediment residues in nearshore marine environments: a critical review. *Rev. Geophys.* 55:1130–57
Hamilton P. 2009. Topographic Rossby waves in the Gulf of Mexico. *Prog. Oceanogr.* 82:1–31
Hasselmann K, Barnett TP, Bouws E, Carlson H, Cartwright DE, et al. 1973. *Measurements of wind-wave growth swell and decay during the Joint North Sea Wave Project (JONSWAP)*. Rep., Dtsch. Hydrogr. Inst., Hamburg, Ger.
Hayes MO, Michel J. 1998. *Evaluation of the condition of Prince William Sound shorelines following the* Exxon Valdez *oil spill and subsequent shoreline treatment: 1997 geomorphological monitoring survey*. Tech. Memo. NOS ORCA 126, Natl. Ocean. Atmos. Adm., Washington, DC

Hayworth JS, Clement TP, Valentine JF. 2011. Deepwater Horizon oil spill impacts on Alabama beaches. *Hydrol. Earth Syst. Sci.* 15:3639–49

Haza AC, D'Asaro E, Chang H, Chen S, Curcic M, et al. 2018. Drogue-loss detection for surface drifters during the Lagrangian Submesoscale Experiment (LASER). *J. Atmos. Ocean. Technol.* 35:705–25

Haza AC, Paldor N, Özgökmen T, Curcic M, Chen SS, Jacobs G. 2019. Wind-based estimations of ocean surface currents from massive clusters of drifters in the Gulf of Mexico. *J. Geophys. Res. Oceans* 124:5844–69

Hazen TC, Prince RC, Mahmoudi N. 2016. Marine oil biodegradation. *Environ. Sci. Technol.* 50:2121–29

Hickey B, Pietrafesa LJ, Jay DA, Boicourt WC. 1998. The Columbia River plume study: subtidal variability in the velocity and salinity fields. *J. Geophys. Res. Oceans* 103:10339–68

Hinze J. 1955. Fundamentals of the hydrodynamic mechanism of splitting in dispersion processes. *AIChE J.* 1:289–95

Hoult DP. 1972. Oil spreading on the sea. *Annu. Rev. Fluid Mech.* 4:341–68

Hu C, Nelson JR, Johns E, Chen Z, Weisberg RH, Müller-Karger FE. 2005. Mississippi River water in the Florida Straits and in the Gulf Stream off Georgia in summer 2004. *Geophys. Res. Lett.* 32:L14606

Ichiye T. 1967. Upper ocean boundary-layer flow determined by dye diffusion. *Phys. Fluids* 10:S270–77

Jacobs GA, Bartels BP, Bogucki DJ, Beron-Vera FJ, Chen SS, et al. 2014. Data assimilation considerations for improved ocean predictability during the Gulf of Mexico Grand Lagrangian Deployment (GLAD). *Ocean Model.* 83:98–117

Ji W, Boufadel MC, Zhao L, Robinson B, King T, Lee K. 2021a. Formation of oil-particle aggregates: particle penetration and impact of particle properties and particle-to-oil concentration ratios. *Sci. Total Environ.* 760:144047

Ji W, Boufadel MC, Zhao L, Robinson B, King T, et al. 2021b. Formation of oil-particle aggregates: impact of mixing energy and duration. *Sci. Total Environ.* 795:148781

Jirka GH. 2004. Integral model for turbulent buoyant jets in unbounded stratified flows. Part I: single round jet. *Environ. Fluid Mech.* 4:1–56

Johansen Ø. 2003. Development and verification of deep-water blowout models. *Mar. Pollut. Bull.* 47:360–68

Johansen Ø, Brandvik PJ, Farooq U. 2013. Droplet breakup in subsea oil releases – part 2: predictions of droplet size distributions with and without injection of chemical dispersants. *Mar. Pollut. Bull.* 73:327–35

Johansen Ø, Rye H, Cooper C. 2003. DeepSpill—field study of a simulated oil and gas blowout in deep water. *Spill Sci. Technol. Bull.* 8:433–43

Johnson JA, Edwards DA, Blue D, Morey SJ. 2018. Physical properties of oil-particle aggregate (OPA)-containing sediments. *Soil Sediment Contam.* 27:706–22

Kourafalou VH, Androulidakis YS. 2013. Influence of Mississippi River induced circulation on the Deepwater Horizon oil spill transport. *J. Geophys. Res. Oceans* 118:3823–42

Kourafalou VH, Oey L-Y Jr., Wang JD, Lee TN. 1996. The fate of river discharge on the continental shelf: 1. Modeling the river plume and the inner shelf coastal current. *J. Geophys. Res. Oceans* 101:3415–34

Langmuir I. 1938. Surface motion of water induced by wind. *Science* 87:119–23

Large WG, McWilliams JC, Doney SC. 1994. Oceanic vertical mixing: a review and a model with a nonlocal boundary layer parameterization. *Rev. Geophys.* 32:363–403

Laxague NJ, Özgökmen TM, Haus BK, Novelli G, Shcherbina A, et al. 2018. Observations of near-surface current shear help describe oceanic oil and plastic transport. *Geophys. Res. Lett.* 45:245–49

Le Hénaff M, Kourafalou VH, Paris CB, Helgers J, Aman ZM, et al. 2012. Surface evolution of the Deepwater Horizon oil spill patch: combined effects of circulation and wind-induced drift. *Environ. Sci. Technol.* 46:7267–73

Ledwell JR, He R, Xue Z, DiMarco SF, Spencer LJ, Chapman P. 2016. Dispersion of a tracer in the deep Gulf of Mexico. *J. Geophys. Res. Oceans* 121:1110–32

Ledwell JR, St. Laurent LC, Girton JB, Toole JM. 2011. Diapycnal mixing in the Antarctic circumpolar current. *J. Phys. Oceanogr.* 41:241–46

Lee JHW, Chu VH. 2003. *Turbulent Jets and Plumes: A Lagrangian Approach*. New York: Springer

Lee K, Boufadel MC, Chen B, Foght J, Hodson P, et al. 2015. *The behaviour and environmental impacts of crude oil released into aqueous environments*. Rep., R. Soc. Can., Ottawa, Can.

Leibovich S. 1983. The form and dynamics of Langmuir circulations. *Annu. Rev. Fluid Mech.* 15:391–427

Li C, Miller J, Wang J, Koley S, Katz J. 2017. Size distribution and dispersion of droplets generated by impingement of breaking waves on oil slicks. *J. Geophys. Res. Oceans* 122:7938–57

Li Z, Spaulding M, McCay DF, Crowley D, Payne JR. 2017. Development of a unified oil droplet size distribution model with application to surface breaking waves and subsea blowout releases considering dispersant effects. *Mar. Pollut. Bull.* 114:247–57

Liu R, Boufadel MC, Zhao L, Nedwed T, Lee K, et al. 2022. Oil droplet formation and vertical transport in the upper ocean. *Mar. Pollut. Bull.* 176:113451

Lodise J, Özgökmen T, Griffa A, Berta M. 2019. Vertical structure of ocean surface currents under high winds from massive arrays of drifters. *Ocean Sci.* 15:1627–51

MacFadyen A, Watabayashi G, Barker C, Beegle-Krause C. 2011. Tactical modeling of surface oil transport during the *Deepwater Horizon* spill response. In *Monitoring and Modeling the* Deepwater Horizon *Oil Spill: A Record-Breaking Enterprise*, ed. Y Liu, A Macfadyen, Z-G Ji, RH Weisberg, pp. 167–78. Washington, DC: Am. Geophys. Soc.

Mackay D, Buist I, Mascaraenhas R, Paterson S. 1980. *Oil spill processes and models*. Rep., Environ. Impact Control Dir., Ottawa, Can.

Mackay D, Chau A, Poon YC. 1986. *A study of the mechanism of chemical dispersion of oil spills*. Rep. EE-93, Environ. Can., Edmonton, Can.

Malone K, Pesch S, Schlüter M, Krause D. 2018. Oil droplet size distributions in deep-sea blowouts: influence of pressure and dissolved gases. *Environ. Sci. Technol.* 52:6326–33

Mariano A, Kourafalou VH, Srinivasan A, Kang H, Halliwell G, et al. 2011. On the modeling of the 2010 Gulf of Mexico oil spill. *Dyn. Atmos. Oceans* 52:322–40

McNutt M, Camilli R, Guthrie G, Hsieh P, Labson V, et al. 2011. *Assessment of flow rate estimates for the Deepwater Horizon/Macondo well oil spill*. Rep., Flow Rate Tech. Group, Interagency Solut. Group, Natl. Incid. Command, US Dep. Interior, Washington, DC

McWilliams JC, Sullivan PP. 2000. Vertical mixing by Langmuir circulations. *Spill Sci. Technol. Bull.* 6:225–37

Mensa JA, Özgökmen TM, Poje AC, Imberger J. 2015. Material transport in a convective surface mixed layer under weak wind forcing. *Ocean Model.* 96:226–42

Michel J, Hayes MO. 1993. *Evaluation of the condition of Prince William Sound shorelines following the Exxon Valdez oil spill and subsequent shoreline treatment, volume I: summary of results—geomorphological shoreline monitoring survey of the Exxon Valdez spill site, Prince William Sound, Alaska, September 1989–August 1992*. Tech. Memo NOS ORCA 73, Natl. Ocean. Atmos. Adm., Washington, DC

Michel J, Owens EH, Zengel S, Graham A, Nixon Z, et al. 2013. Extent and degree of shoreline oiling: *Deepwater Horizon* oil spill, Gulf of Mexico, USA. *PLOS ONE* 8:e65087

Monin AS, Yalgom AM. 1975. Statistical characteristics of wave and turbulent components of the random velocity field in the marine surface layer. In *Statistical Fluid Mechanics: Mechanics of Turbulence*, Vol. 2, pp. 659–66. Cambridge, MA: MIT Press

Murphy DW, Xue X, Sampath K, Katz J. 2016. Crude oil jets in crossflow: effects of dispersant concentration on plume behavior. *J. Geophys. Res. Oceans* 121:4264–81

Nordam T, Nepstad R, Litzler E, Röhrs J. 2019. On the use of random walk schemes in oil spill modelling. *Mar. Pollut. Bull.* 146:631–38

Novelli G, Guigand CM, Boufadel MC, Özgökmen TM. 2020. On the transport and landfall of marine oil spills, laboratory and field observations. *Mar. Pollut. Bull.* 150:110805

Novelli G, Guigand CM, Cousin C, Ryan EH, Laxague NJ, et al. 2017. A biodegradable surface drifter for ocean sampling on a massive scale. *J. Atmos. Ocean. Technol.* 34:2509–32

NRC (Natl. Res. Counc.). 2013. *An Ecosystem Services Approach to Assessing the Impacts of the* Deepwater Horizon *Oil Spill in the Gulf of Mexico*. Washington, DC: Natl. Acad. Press

NRC (Natl. Res. Counc.). 2019. *The Use of Dispersants in Marine Oil Spill Response*. Washington, DC: Natl. Acad. Press

Nummelin A, Busecke JJ, Haine TW, Abernathey RP. 2021. Diagnosing the scale-and space-dependent horizontal eddy diffusivity at the global surface ocean. *J. Phys. Oceanogr.* 51:279–97

Oey L-Y Jr., Ezer T, Lee H-C. 2005. Loop Current, rings and related circulation in the Gulf of Mexico: a review of numerical models and future challenges. In *Circulation in the Gulf of Mexico: Observations and Models*, ed. W Sturges, A Lugo-Fernandez, pp. 31–56. Washington, DC: Am. Geophys. Union

Oey L-Y Jr., Lee H-C. 2002. Deep eddy energy and topographic Rossby waves in the Gulf of Mexico. *J. Phys. Oceanogr.* 32:3499–527

Okubo A. 1971. Oceanic diffusion diagrams. *Deep-Sea Res. Oceanogr. Abstr.* 18:789–802

OSAT-2 (Oper. Sci. Adv. Team 2). 2011. *Summary report for fate and effects of remnant oil in the beach environment*. Rep., OSAT-2. **https://www.restorethegulf.gov/sites/default/files/u316/OSAT-2%20Report%20no%20ltr.pdf**

OSAT-3 (Oper. Sci. Adv. Team 3). 2013. *Investigation of recurring residual oil in discrete shoreline areas in the eastern area of responsibility*. Rep., OSAT-3. **https://www.restorethegulf.gov/sites/default/files/u372/OSAT%20III%20Eastern%20States.pdf**

Owens EH, Sergy GA. 2000. *The SCAT Manual: A Field Guide to the Documentation and Description of Oiled Shorelines*. Edmonton: Environ. Can.

Özgökmen TM, Boufadel MC, Carlson DF, Cousin C, Guigand C, et al. 2018. Technological advances for ocean surface measurements by the Consortium for Advanced Research on Transport of Hydrocarbons in the Environment (CARTHE). *Mar. Technol. Soc. J.* 52:71–76

Özgökmen TM, Chassignet EP, Dawson CN, Dukhovskoy D, Jacobs G, et al. 2016. Over what area did the oil and gas spread during the 2010 Deepwater Horizon oil spill? *Oceanography* 29(3):96–107

Paris CB, Le Hénaff M, Aman ZM, Subramaniam A, Helgers J, et al. 2012. Evolution of the Macondo well blowout: simulating the effects of the circulation and synthetic dispersants on the subsea oil transport. *Environ. Sci. Technol.* 46:13293–302

Passow U, Overton EB. 2021. The complexity of spills: the fate of the *Deepwater Horizon* oil. *Annu. Rev. Mar. Sci.* 13:109–36

Pesch S, Jaeger P, Jaggi A, Malone K, Hoffmann M, et al. 2018. Rise velocity of live-oil droplets in deep-sea oil spills. *Environ. Eng. Sci.* 35:289–99

Pesch S, Schlüter M, Aman ZM, Malone K, Krause D, Paris CB. 2020. Behavior of rising droplets and bubbles: impact on the physics of deep-sea blowouts and oil fate. In *Deep Oil Spills*, ed. SA Murawski, CH Ainsworth, S Gilbert, DJ Hollander, CB Paris, et al., pp. 65–82. Cham, Switz.: Springer

Phillips O. 1958. The equilibrium range in the spectrum of wind-generated waves. *J. Fluid Mech.* 4:426–34

Plant NG, Long JW, Dalyander PS, Thompson DM, Raabe EA. 2012. *Application of a hydrodynamic and sediment transport model for guidance of response efforts related to the Deepwater Horizon oil spill in the Northern Gulf of Mexico along the coast of Alabama and Florida*. Open-File Rep. 2012-1234, US Geol. Surv., Washington DC

Prince RC, McFarlin KM, Butler JD, Febbo EJ, Wang FC, Nedwed TJ. 2013. The primary biodegradation of dispersed crude oil in the sea. *Chemosphere* 90:521–26

Reddy CM, Arey JS, Seewald JS, Sylva SP, Lemkau KL, et al. 2012. Composition and fate of gas and oil released to the water column during the *Deepwater Horizon* oil spill. *PNAS* 109:20229–34

Richardson LF. 1926. Atmospheric diffusion shown on a distance-neighbour graph. *Proc. R. Soc. Lond. A* 110:709–37

Ryerson TB, Aikin K, Angevine W, Atlas EL, Blake D, et al. 2011. Atmospheric emissions from the Deepwater Horizon spill constrain air-water partitioning, hydrocarbon fate, and leak rate. *Geophys. Res. Lett.* 38:L07803

Ryerson TB, Camilli R, Kessler JD, Kujawinski EB, Reddy CM, et al. 2012. Chemical data quantify *Deepwater Horizon* hydrocarbon flow rate and environmental distribution. *PNAS* 109:20246–53

Schiller RV, Kourafalou VH. 2010. Modeling river plume dynamics with the HYbrid Coordinate Ocean Model. *Ocean Model.* 33:101–17

Schiller RV, Kourafalou VH, Hogan P, Walker N. 2011. The dynamics of the Mississippi River plume: impact of topography, wind and offshore forcing on the fate of plume waters. *J. Geophys. Res. Oceans* 116:C06029

Schwendeman M, Thomson J, Gemmrich JR. 2014. Wave breaking dissipation in a young wind sea. *J. Phys. Oceanogr.* 44:104–27

Short JW, Geiger HJ, Haney JC, Voss CM, Vozzo ML, et al. 2017. Anomalously high recruitment of the 2010 Gulf menhaden (*Brevoortia patronus*) year class: evidence of indirect effects from the *Deepwater Horizon* blowout in the Gulf of Mexico. *Arch. Environ. Contam. Toxicol.* 73:76–92

Simecek-Beatty D, Lehr WJ. 2017. Extended oil spill spreading with Langmuir circulation. *Mar. Pollut. Bull.* 122:226–35

Smith C, Li Z, Tejada-Martinez A, Murphy D. 2019. Oil droplet and sediment suspension in laboratory-scale Stommel retention zones. *Bull. Am. Phys. Soc.* 64:M02.00049 (Abstr.)

Socolofsky SA, Adams EE. 2002. Multi-phase plumes in uniform and stratified crossflow. *J. Hydraul. Res.* 40:661–72

Socolofsky SA, Adams EE. 2005. Role of slip velocity in the behavior of stratified multiphase plumes. *J. Hydraul. Eng.* 131:273–82

Socolofsky SA, Adams EE, Sherwood CR. 2011. Formation dynamics of subsurface hydrocarbon intrusions following the Deepwater Horizon blowout. *Geophys. Res. Lett.* 38:L09602

Socolofsky SA, Bhaumik T, Seol D-G. 2008. Double-plume integral models for near-field mixing in multiphase plumes. *J. Hydraul. Eng.* 134:772–83

Spaulding ML. 2017. State of the art review and future directions in oil spill modeling. *Mar. Pollut. Bull.* 115:7–19

Taylor E, Reimer D. 2008. Oil persistence on beaches in Prince William Sound – a review of SCAT surveys conducted from 1989 to 2002. *Mar. Pollut. Bull.* 56:458–74

Thorpe SA. 1984. The effect of Langmuir circulation on the distribution of submerged bubbles caused by breaking wind waves. *J. Fluid Mech.* 142:151–70

Tobin T, Muralidhar R, Wright H, Ramkrishna D. 1990. Determination of coalescence frequencies in liquid–liquid dispersions: effect of drop size dependence. *Chem. Eng. Sci.* 45:3491–504

Townsend AA. 1980. *The Structure of Turbulent Shear Flow*. Cambridge, UK: Cambridge Univ. Press

Turner J. 1986. Turbulent entrainment: the development of the entrainment assumption, and its application to geophysical flows. *J. Fluid Mech.* 173:431–71

Valentine DL, Fisher GB, Bagby SC, Nelson RK, Reddy CM, et al. 2014. Fallout plume of submerged oil from *Deepwater Horizon*. *PNAS* 111:15906–11

Valentine DL, Kessler JD, Redmond MC, Mendes SD, Heintz MB, et al. 2010. Propane respiration jump-starts microbial response to a deep oil spill. *Science* 330:208–11

Vaz AC, Faillettaz R, Paris CB. 2021. A coupled Lagrangian-Earth system model for predicting oil photooxidation. *Front. Mar. Sci.* 8:576747

Visser AW. 1997. Using random walk models to simulate the vertical distribution of particles in a turbulent water column. *Mar. Ecol. Prog. Ser.* 158:275–81

Walker ND, Huh OK, Rouse LJ Jr., Murray SP. 1996. Evolution and structure of a coastal squirt off the Mississippi River delta: northern Gulf of Mexico. *J. Geophys. Res. Oceans* 101:20643–55

Walker ND, Pilley CT, Raghunathan VV, D'Sa EJ, Leben RR, et al. 2011. Impacts of Loop Current frontal cyclonic eddies and wind forcing on the 2010 Gulf of Mexico oil spill. In *Monitoring and Modeling the* Deepwater Horizon *Oil Spill: A Record-Breaking Enterprise*, ed. Y Liu, A Macfadyen, Z-G Ji, RH Weisberg, pp. 103–16. Washington, DC: Am. Geophys. Soc.

Wang B, Jun I, Socolofsky SA, DiMarco SF, Kessler JD. 2020. Dynamics of gas bubbles from a submarine hydrocarbon seep within the hydrate stability zone. *Geophys. Res. Lett.* 47:e2020GL089256

Wang B, Socolofsky SA, Breier JA, Seewald JS. 2016. Observations of bubbles in natural seep flares at MC 118 and GC 600 using in situ quantitative imaging. *J. Geophys. Res. Oceans* 121:2203–30

Wang P, Özgökmen T. 2018. Langmuir circulation with explicit surface waves from moving-mesh modeling. *Geophys. Res. Lett.* 45:216–26

Ward CP, Sharpless CM, Valentine DL, French-McCay DP, Aeppli C, et al. 2018. Partial photochemical oxidation was a dominant fate of *Deepwater Horizon* surface oil. *Environ. Sci. Technol.* 52:1797–805

Warzinski RP, Lynn R, Haljasmaa I, Leifer I, Shaffer F, et al. 2014. Dynamic morphology of gas hydrate on a methane bubble in water: observations and new insights for hydrate film models. *Geophys. Res. Lett.* 41:6841–47

Webb A, Fox-Kemper B. 2015. Impacts of wave spreading and multidirectional waves on estimating Stokes drift. *Ocean Model.* 96:49–64

Welsh SE, Inoue M. 2000. Loop Current rings and the deep circulation in the Gulf of Mexico. *J. Geophys. Res. Oceans* 105:16951–59

Wu J. 1983. Sea-surface drift currents induced by wind and waves. *J. Phys. Oceanogr.* 13:1441–51

Yang D, Chamecki M, Meneveau C. 2014. Inhibition of oil plume dilution in Langmuir ocean circulation. *Geophys. Res. Lett.* 41:1632–38

Zhao L, Boufadel MC, Adams EE, Socolofsky SA, King T, Lee K. 2015. Simulation of scenarios of oil droplet formation from the Deepwater Horizon blowout. *Mar. Pollut. Bull.* 101:304–19

Zhao L, Boufadel MC, Geng X, Lee K, King T, et al. 2016. A-DROP: a predictive model for the formation of oil particle aggregates (OPAs). *Mar. Pollut. Bull.* 106:245–59

Zhao L, Boufadel MC, Katz J, Haspel G, Lee K, et al. 2017a. A new mechanism of sediment attachment to oil in turbulent flows: projectile particles. *Environ. Sci. Technol.* 51:11020–28

Zhao L, Boufadel MC, King T, Robinson B, Gao F, et al. 2017b. Droplet and bubble formation of combined oil and gas releases in subsea blowouts. *Mar. Pollut. Bull.* 120:203–16

Zhao L, Boufadel MC, Socolofsky SA, Adams E, King T, Lee K. 2014. Evolution of droplets in subsea oil and gas blowouts: development and validation of the numerical model VDROP-J. *Mar. Pollut. Bull.* 83:58–69

Zhao L, Mitchell DA, Prince RC, Walker AH, Arey JS, Nedwed TJ. 2021. Deepwater Horizon 2010: Subsea dispersants protected responders from VOC exposure. *Mar. Pollut. Bull.* 173:113034

Zheng L, Yapa PD. 2000. Buoyant velocity of spherical and nonspherical bubbles/droplets. *J. Hydraul. Eng.* 126:852–54